

High-Temperature Creep of Carbon Yarns and Composites

Prepared by
L. A. FELDMAN
Materials Sciences Laboratory
Laboratory Operations

30 September 1987

Prepared for
OFFICE OF NAVAL RESEARCH
Arlington, VA 22217

SPACE DIVISION
AIR FORCE SYSTEMS COMMAND
Los Angeles Air Force Station
P.O. Box 92960, Worldway Postal Center
Los Angeles, CA 90009-2960

DEPARTMENT OF DEFENSE
ELASTICS TECHNICAL EVALUATION CENTER
WARRACOM, DOVER, N. J. 07801

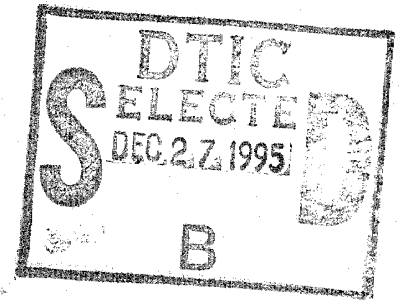
Contract No. F04701-85-C-0086

Laboratory Operations

THE AEROSPACE CORPORATION

APPROVED FOR PUBLIC RELEASE; DISTRIBUTION UNLIMITED.

DTIC QUALITY INSPECTED L



19951218 034

PLAS
4
51339

LABORATORY OPERATIONS

The Aerospace Corporation functions as an "architect-engineer" for national security projects, specializing in advanced military space systems. Providing research support, the corporation's Laboratory Operations conducts experimental and theoretical investigations that focus on the application of scientific and technical advances to such systems. Vital to the success of these investigations is the technical staff's wide-ranging expertise and its ability to stay current with new developments. This expertise is enhanced by a research program aimed at dealing with the many problems associated with rapidly evolving space systems. Contributing their capabilities to the research effort are these individual laboratories:

Aerophysics Laboratory: Launch vehicle and reentry fluid mechanics, heat transfer and flight dynamics; chemical and electric propulsion, propellant chemistry, chemical dynamics, environmental chemistry, trace detection; spacecraft structural mechanics, contamination, thermal and structural control; high temperature thermomechanics, gas kinetics and radiation; cw and pulsed chemical and excimer laser development including chemical kinetics, spectroscopy, optical resonators, beam control, atmospheric propagation, laser effects and countermeasures.

Chemistry and Physics Laboratory: Atmospheric chemical reactions, atmospheric optics, light scattering, state-specific chemical reactions and radiative signatures of missile plumes, sensor out-of-field-of-view rejection, applied laser spectroscopy, laser chemistry, laser optoelectronics, solar cell physics, battery electrochemistry, space vacuum and radiation effects on materials, lubrication and surface phenomena, thermionic emission, photo-sensitive materials and detectors, atomic frequency standards, and environmental chemistry.

Computer Science Laboratory: Program verification, program translation, performance-sensitive system design, distributed architectures for spaceborne computers, fault-tolerant computer systems, artificial intelligence, micro-electronics applications, communication protocols, and computer security.

Electronics Research Laboratory: Microelectronics, solid-state device physics, compound semiconductors, radiation hardening; electro-optics, quantum electronics, solid-state lasers, optical propagation and communications; microwave semiconductor devices, microwave/millimeter wave measurements, diagnostics and radiometry, microwave/millimeter wave thermionic devices; atomic time and frequency standards; antennas, rf systems, electromagnetic propagation phenomena, space communication systems.

Materials Sciences Laboratory: Development of new materials: metals, alloys, ceramics, polymers and their composites, and new forms of carbon; non-destructive evaluation, component failure analysis and reliability; fracture mechanics and stress corrosion; analysis and evaluation of materials at cryogenic and elevated temperatures as well as in space and enemy-induced environments.

Space Sciences Laboratory: Magnetospheric, auroral and cosmic ray physics, wave-particle interactions, magnetospheric plasma waves; atmospheric and ionospheric physics, density and composition of the upper atmosphere, remote sensing using atmospheric radiation; solar physics, infrared astronomy, infrared signature analysis; effects of solar activity, magnetic storms and nuclear explosions on the earth's atmosphere, ionosphere and magnetosphere; effects of electromagnetic and particulate radiations on space systems; space instrumentation.

*MSG DIA DROLS PROCESSING - LAST INPUT IGNORED

-- 1 OF 3

OTIC DOES NOT HAVE THIS ITEM

-- 1 - AD NUMBER: D852231

-- 5 - CORPORATE AUTHOR: AEROSPACE CORP EL SEGUNDO CA MATERIALS SCIENCES
LAB

-- 6 - UNCLASSIFIED TITLE: HIGH-TEMPERATURE CREEP OF CARBON YARNS AND
COMPOSITES.

-- 9 - DESCRIPTIVE NOTE: TECHNICAL REPT., 30 SEP 87,

--10 - PERSONAL AUTHORS: FELDMAN, L. A.

--11 - REPORT DATE: , 1987

--12 - PAGINATION: 65P

--14 - REPORT NUMBER: TOR-0086(6728-02)-2

--15 - CONTRACT NUMBER: F04701-85-C-0086

--20 - REPORT CLASSIFICATION: UNCLASSIFIED

--21 - SUPPLEMENTARY NOTE: AD-D441 537.

--22 - LIMITATIONS (ALPHA):

--33 - LIMITATION CODES: 1

(NOT AVAILABLE FROM DTIC)

UNCLASSIFIED

SECURITY CLASSIFICATION OF THIS PAGE

REPORT DOCUMENTATION PAGE

1a. REPORT SECURITY CLASSIFICATION Unclassified			1b. RESTRICTIVE MARKINGS		
2a. SECURITY CLASSIFICATION AUTHORITY			3. DISTRIBUTION / AVAILABILITY OF REPORT Approved for public release; distribution unlimited.		
2b. DECLASSIFICATION / DOWNGRADING SCHEDULE					
4. PERFORMING ORGANIZATION REPORT NUMBER(S) TOR-0086(6728-02)-2			5. MONITORING ORGANIZATION REPORT NUMBER(S)		
6a. NAME OF PERFORMING ORGANIZATION The Aerospace Corporation Laboratory Operations		6b. OFFICE SYMBOL (If applicable)	7a. NAME OF MONITORING ORGANIZATION Office of Naval Research		
6c. ADDRESS (City, State, and ZIP Code) El Segundo, CA 90245			7b. ADDRESS (City, State, and ZIP Code) Arlington, VA 22217		
8a. NAME OF FUNDING / SPONSORING ORGANIZATION Space Division		8b. OFFICE SYMBOL (If applicable)	9. PROCUREMENT INSTRUMENT IDENTIFICATION NUMBER F04701-85-C-0086		
8c. ADDRESS (City, State, and ZIP Code) Los Angeles Air Force Station Los Angeles, CA 90009-2960			10. SOURCE OF FUNDING NUMBERS		
			PROGRAM ELEMENT NO.	PROJECT NO.	TASK NO.
					WORK UNIT ACCESSION NO.
11. TITLE (Include Security Classification) High-Temperature Creep of Carbon Yarns and Composites					
12. PERSONAL AUTHOR(S) Feldman, Leslie A.					
13a. TYPE OF REPORT		13b. TIME COVERED FROM _____ TO _____		14. DATE OF REPORT (Year, Month, Day) 1987 September 30	
15. PAGE COUNT 54					
16. SUPPLEMENTARY NOTATION					
17. COSATI CODES			18. SUBJECT TERMS (Continue on reverse if necessary and identify by block number)		
FIELD	GROUP	SUB-GROUP	Activation energy Carbon yarns		
			Carbon-carbon composites Creep		
			Carbon fibers High-temperature creep		
19. ABSTRACT (Continue on reverse if necessary and identify by block number)					
<p>Effects of creep and deformation at high temperatures in carbon-carbon composites have been investigated. High-temperature creep in composites may play an important role in processing, through relaxation of thermally induced stresses caused by thermal expansion anisotropy of graphite. Creep has been measured in unidirectional composites at temperatures between 2000 and 3000°C.</p> <p>Various distinctions have been observed among the creep behaviors of composites utilizing PAN-, rayon-, and mesophase-pitch-based carbon fibers, such as decreasing creep rates and elongations with increasing stiffness and degree of graphitic disorder. Fiber-matrix debonding at high temperature, such as that in microstructural observations using SEM, occurs after high-temperature deformation and is visible in the interior of microcracks and at fracture ends. Estimates of relative thermal expansion coefficients of different fiber composites under low stress in the creep regime have been obtained from</p>					
20. DISTRIBUTION / AVAILABILITY OF ABSTRACT <input checked="" type="checkbox"/> UNCLASSIFIED/UNLIMITED <input type="checkbox"/> SAME AS RPT. <input type="checkbox"/> DTIC USERS			21. ABSTRACT SECURITY CLASSIFICATION Unclassified		
22a. NAME OF RESPONSIBLE INDIVIDUAL			22b. TELEPHONE (Include Area Code)		22c. OFFICE SYMBOL

18. SUBJECT TERMS (Continued)

Microstructure
 Nonuniform temperature distribution
 Pitch matrices
 Resistance ratio measurements
 Vibrational modulus

Dynamic modulus measurements

19. ABSTRACT (Continued)

rapid-heating-rate experiments (where $\alpha \dot{T} \approx \dot{\epsilon}_{\text{thermal}} \gg \dot{\epsilon}_{\text{creep}}$), and are lower for more highly oriented fibers. Vibrational modulus measurements and resistance ratio measurements have also been used to assess composite modulus, fiber utilization efficiency, and various creep-induced changes in properties.

Accession For	
WHS CRAL	<input checked="" type="checkbox"/>
WHS LAD	<input type="checkbox"/>
Uncovered	<input type="checkbox"/>
Justification	
<i>Printout enclosed</i>	
<i>27 Oct 72</i>	
Distribution	
Available Under	
Basic	Special
<i>A-1</i>	


HIGH-TEMPERATURE CREEP OF CARBON YARNS
AND COMPOSITES

Prepared

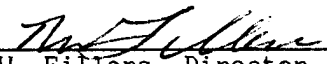


L. A. Feldman

Approved



H. A. Katzman, Head
Carbon and Polymers Department



R. W. Fillers, Director
Materials Sciences Laboratory

The information in a Technical Operating Report is developed for a particular program and is therefore not necessarily of broader technical applicability.

ACKNOWLEDGMENTS

This work was supported by the Office of Naval Research under the direction of Dr. L. H. Peebles. The author thanks Prof. G. Sines of the University of California at Los Angeles and Drs. R. A. Meyer, H. A. Katzman, G. S. Rellick, M. A. Piliavin, D. J. Chang, J. L. White, and G. A. Binegar for helpful technical discussions. The excellent technical assistance of D. C. Robinson and H. G. Hoppe is also acknowledged.

CONTENTS

ACKNOWLEDGMENTS.....	v
I. INTRODUCTION.....	1
II. EXPERIMENTAL.....	3
III. ANALYSIS AND DISCUSSION.....	5
A. CREEP OBSERVATIONS.....	5
1. WCA/A240 Composite.....	5
2. P55/A240 Composite.....	7
3. HM3000/15V Composite.....	7
B. VARIABILITY OF CREEP.....	13
C. THERMAL EXPANSION EFFECTS.....	18
1. Measurements.....	18
2. Variation of Thermal Expansion Coefficients--Discussion.....	22
D. VIBRATIONAL MODULUS.....	24
E. ELECTRICAL RESISTANCE PROPERTIES.....	26
IV. DISCUSSION AND CONCLUSION.....	29
V. SUMMARY.....	33
REFERENCES.....	35
APPENDICES	
A. DESCRIPTION OF EXPERIMENTAL APPARATUS.....	37
B. MEASUREMENTS OF FIBER AND COMPOSITE MODULI BY A MECHANICAL VIBRATION TECHNIQUE.....	43
C. RESISTIVITY AND RELATIVE RESISTANCE MEASUREMENTS ON CARBON FILAMENTS.....	49

FIGURES

1.	Schematic Description of High-Temperature Creep Furnace.....	4
2.	Schematic Description of Variable Load Device.....	4
3.	Plots of Creep Data from Low to High Temperature and Activation Energy, for WCA/A240 Composites.....	8
4.	Plots of Creep Data from Low to High Temperature and Activation Energy, for P55/A240 Composites.....	9
5.	Photomicrograph of Failed End of P55/A240 Specimen, Showing Slight Filament Necking.....	10
6.	Plots of Creep Data from Low to High Temperature and Activation Energy, for HM3000/15V Composites.....	11
7.	Photomicrographs of Failed End of HM3000/15V Specimen, Showing Filament Necking and Matrix Shrinkage Cracks.....	12
8.	Photomicrographs of Surface Geometry of P55 (Round) and WCA (Crenulated) Carbon Filaments (As-received), for Comparison.....	16

TABLES

1.	Creep Elongation of WCA/A240.....	6
2.	WCA/A240 Thermal Expansion.....	20
3.	P55/A240 Thermal Expansion.....	21
4.	HM3000/15V Thermal Expansion.....	21
5.	Relative Differences in CTE.....	23
6.	Vibrating Beam Technique Results for Unidirectional Composites.....	25

I. INTRODUCTION

Carbon-carbon composites are used in such applications as rocket engine throat inserts and exit cones, which require light weight and strength at extremely high temperatures. They are an arrangement of carbon fibers (typically 2-D or 3-D reinforcement) infiltrated with a carbonaceous matrix (either graphitized or amorphous, depending on the matrix precursor and processing parameters). Graphite's high degree of anisotropy parallel and perpendicular to the basal plane can generate large thermal stresses within the composite during processing to high temperature, and those stresses can cause damage and defects in the structure during processing (Sines and Cohen, 1982).

One aspect of high-temperature processing that has been insufficiently explored is the effect of creep, or time-dependent deformation under load, on stress relaxation in composites. This report continues the investigation of high-temperature creep effects in carbon yarns and unidirectional carbon-carbon composites (i.e., carbon yarns with carbonized, pitch-derived matrices) reported on previously (Feldman, 1983, 1985), an effort to measure creep rates and elongations to failure at high temperature in unimpregnated yarns and composites. This work describes experimental modifications and comparisons of high-temperature creep elongation behavior in different unidirectional composites. Such creep behavior is affected by a number of factors, including fiber type, matrix precursor, and fiber-matrix debonding. These factors, as well as changes in properties caused by creep, have been studied using a dynamic modulus measurement technique, which measures vibrational resonance of the sample. From the resonance, one can determine an apparent, or effective, modulus for the sample, which can be related to changes induced by creep, such as changes in interfacial bonding or matrix properties. To try to understand changes in the materials at high temperature, measurements have been performed to determine the fibers' resistance ratio, the ratio of resistance at 300 and 77 K in a single sample, which has been considered a form of "graphitic order parameter" (see Robson et al., 1973). That information should enable the effects of heat treatment and creep on fibers and composites to be assessed separately.

II. EXPERIMENTAL

Materials used in fabrication of unidirectional composites were P55 mesophase pitch yarns (Union Carbide), WCA rayon-based cloth yarn (Union Carbide) and HM3000 polyacrylonitrile (PAN) yarns (Hercules), and A240 petroleum pitch (Ashland) and 15V coal-tar pitch (Allied). Composites were fabricated by passing a continuous yarn through a bath of molten pitch in a furnace under an inert atmosphere. The impregnated yarn was then calcined to 1000°C under inert atmosphere (Feldman, 1985). Microstructural examination of the samples was conducted using standard experimental techniques, such as optical microscopy and scanning electron microscopy (SEM). The high-temperature creep furnace for the experiments is shown schematically in Fig. 1. The temperature is measured by an optical pyrometer, and displacement of one end of the sample is measured with a linear variable differential transformer (LVDT) with an output sensitivity of 0.099 V/mm. The load on the sample is controlled automatically by a dc solenoid (Fig. 2), which enables both stress and temperature variables in the material to be controlled. A more detailed description of the experimental apparatus is given in Appendix A.

Elastic properties were determined by a dynamic modulus measurement technique that measured changes in the sample elastic modulus caused by creep and heat treatment. Measurements are made by determining the mechanical resonance frequency of the sample while an ac current is being passed through the sample in the presence of a magnetic field. The method, discussed in Appendix B, has provided an additional means of characterizing the samples and the effects of creep- or processing-variable-induced changes in the microstructure. Measurements have also been made of the changes in certain electrical properties, particularly the resistance ratio at 77 and 300 K of carbon fibers before and after heat treatment and with and without high-temperature creep, by mounting samples on a resistance measurement jig and using a two-probe resistance measurement on the sample at room temperature and after immersion in liquid nitrogen (discussed in Appendix C).

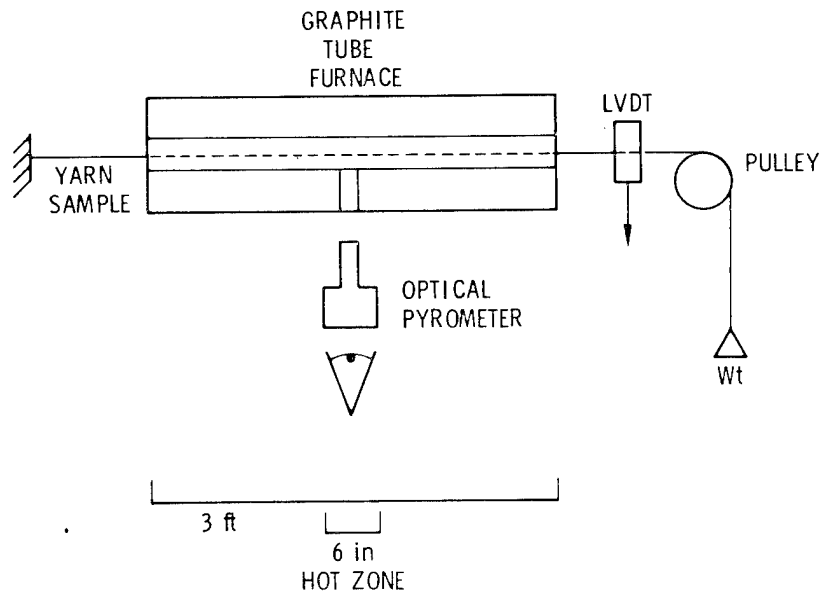


Fig. 1. Schematic Description of High-Temperature Creep Furnace

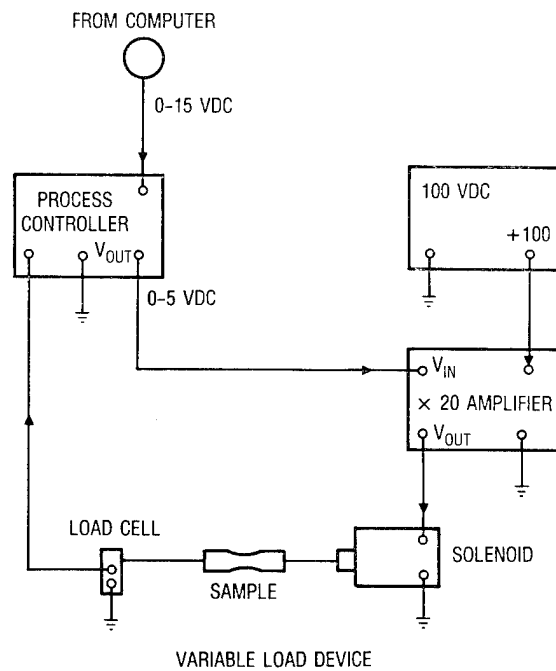


Fig. 2. Schematic Description of Variable Load Device

III. ANALYSIS AND DISCUSSION

A. CREEP OBSERVATIONS

Particular impregnated carbon yarn composites will be referred to here as "fiber/matrix." For example, WCA/A240 indicates a composite of WCA yarn and a matrix produced from A240 pitch. Samples of composites of WCA/A240, P55/A240, and HM3000/15V were analyzed for total strain to failure between 2000 and 3000°C. An interpretation is proposed for thermal expansion of the composites under load during rapid heating at creep temperatures.

1. WCA/A240 COMPOSITE

Total sample elongation consists of a thermal expansion term and a creep term as follows:

$$\Delta L_{\text{total}} = \Delta L_{\text{thermal}} + \Delta L_{\text{creep}} \quad (1)$$

The elongation rate is then

$$(d/dt)\Delta L_{\text{total}} = (d/dt)\Delta L_{\text{thermal}} + (d/dt)\Delta L_{\text{creep}} \quad (2)$$

During the isothermal portions of the creep experiment, the creep rate contribution to the total elongation rate was constant, and the thermal expansion contribution was zero. Thus, assuming an approximate gage length, L_{gl} , for creep of 15.2 cm (6 in.), corresponding to the furnace hot-zone length, creep strain during isothermal periods was obtained from $\Delta L_{\text{total}}/L_{gl}$ (Feldman, 1985).

A calculation of creep strain to failure of a WCA/A240 composite over the temperature range 2100 to 2750°C is given in Table 1. Incremental creep strains are determined from LVDT data for isothermal periods, typically 0.5 to 1 hr. Incremental strains during periods of rapid temperature change (~ 3-4 min) between isothermal periods are neglected; they are ascribed mainly to thermal expansion (Feldman, 1983). Table 1 indicates a net elongation due

Table 1. Creep Elongation of WCA/A240

Time	Temperature, °C	Weight, g	LVDT, V
3:00	2100	173	1.6269
4:11:15			1.6786
4:26:15	2100	173	1.7533
5:07:30			1.8168
5:15	2200	173	1.9378
5:45			2.1397
5:56:15	2260	173	2.3863
6:41:15			2.6282
7:18:45	2420	173	3.3650
7:45			3.6547
7:52:30	2350	223	3.6513
8:52:30			3.7660
9:00	2270	273	3.7860
9:26:15			3.7979
9:45	2430	173	0.4739
9:56:15			0.4927
10:00	2390	223	0.5114
10:15			0.5305
10:22:30	2250	273	0.5550
10:37:30			0.5708
10:45	2390	173	0.5822
11:11:15			0.6303
11:22:30	2500	173	0.7982
11:48:45			1.0546
12:00	2630	173	1.4943
12:41:15			2.7252
12:52:30	2750	173	3.5297
13:11:15			4.0817

NOTE: Total change due to creep: 20.7% (LVDT change:
3.1164 V, 31.48 mm; calibration: 0.099 V/mm).

to creep of 20.7% over the gage length for WCA/A240 composite yarn (see also Fig. 3). Localized necking, or decrease in fiber diameter, near the point at which the composite fractures indicates that local strains may be higher. Localized necking is not reflected in the total creep elongation, because it affects only a small region near the failure point; consequently, most of the overall elongation is produced by more uniform strain over a longer length of material.

2. P55/A240 COMPOSITE

For the P55/A240 sample, the net elongation due to creep was 2.6%. An example of elongation as a function of time is presented in Fig. 4, together with an example of creep behavior of an unimpregnated P55 yarn, for two heating and creep cycles. As for WCA/A240, there is some localized necking near the point of composite fracture, but it does not contribute significantly to the total creep strain. An example of a region near the point of failure of a P55/A240 sample is shown in Fig. 5.

3. HM3000/15V COMPOSITE

Creep strains to failure for an HM3000/15V composite over the temperature range of 2500 to 2700°C are plotted in Fig. 6. Experimental conditions were similar to those for the WCA/A240 sample. The net elongation caused by creep was 1.3% over the gage length for the composite yarn. The run was performed in two stages: Creep was measured in the first run up to a temperature of 2700°C; the temperature was decreased to 2000°C, and the run was repeated. Creep was unmeasurable until a temperature of 2780°C was reached. Very little tertiary creep was observed before sample failure, which occurred during the last temperature ramp beyond 2945°C, at approximately 3050°C. The total elongation to failure was computed by combining the elongations from both runs, 0.401 mm from the first and 1.96 mm from the second. There is some localized necking near the point of composite fracture, but it does not contribute significantly to the total creep strain. An example of a region near the point of failure of an HM3000/15V sample is shown in Fig. 7, which depicts a creep-induced enlargement of transverse matrix cracks, and necking of HM3000 filaments within the cracks.

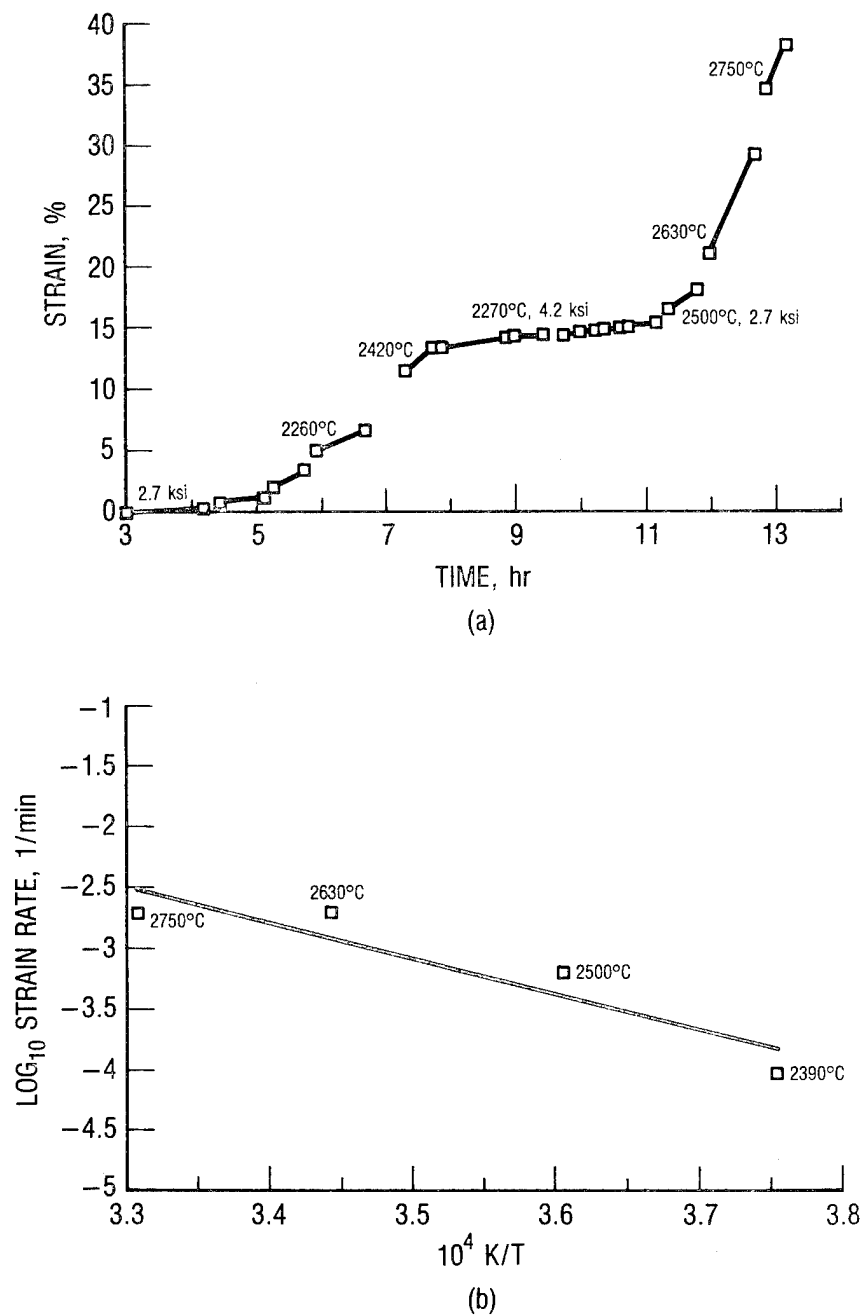


Fig. 3. Plots of (a) Creep Data from Low to High Temperature and (b) Activation Energy, for WCA/A240 Composites

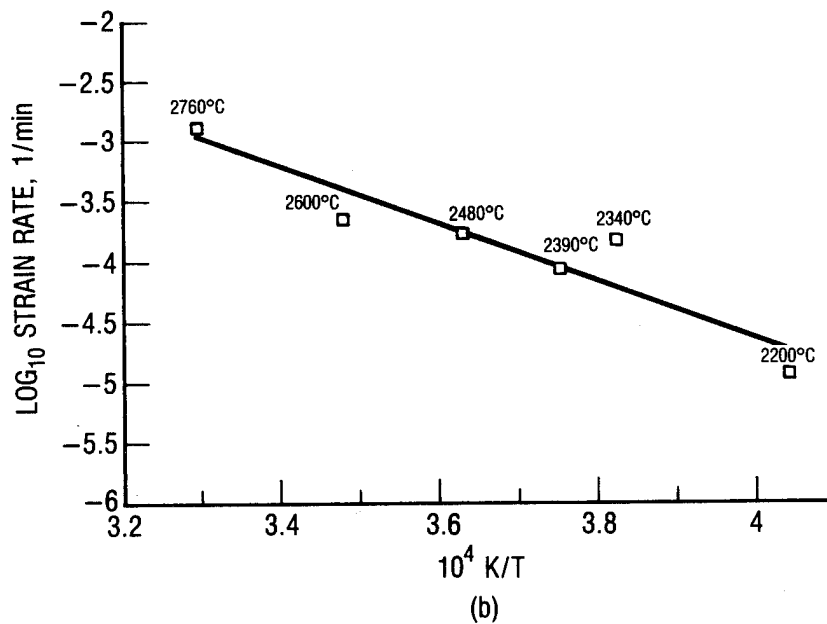
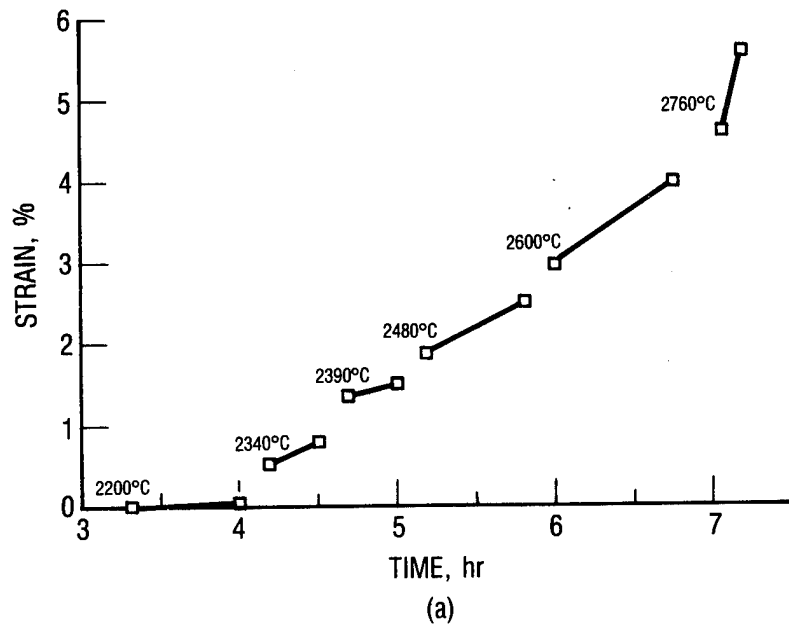
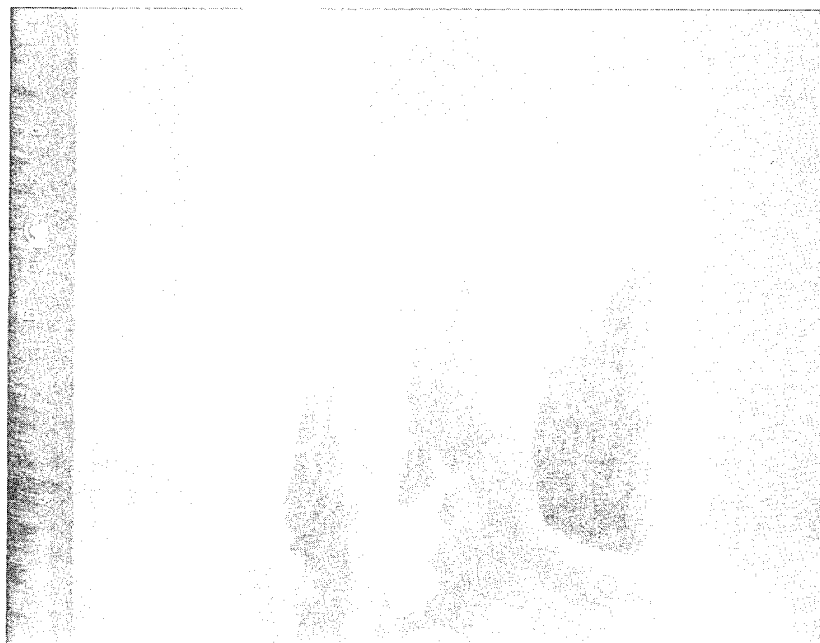


Fig. 4. Plots of (a) Creep Data from Low to High Temperature and (b) Activation Energy, for P55/A240 Composites



5 μm

Fig. 5. Photomicrograph of Failed End of P55/A240 Specimen, Showing Slight Filament Necking. Fracture extends over region of limited size, indicating small effective shear stress redistribution length.

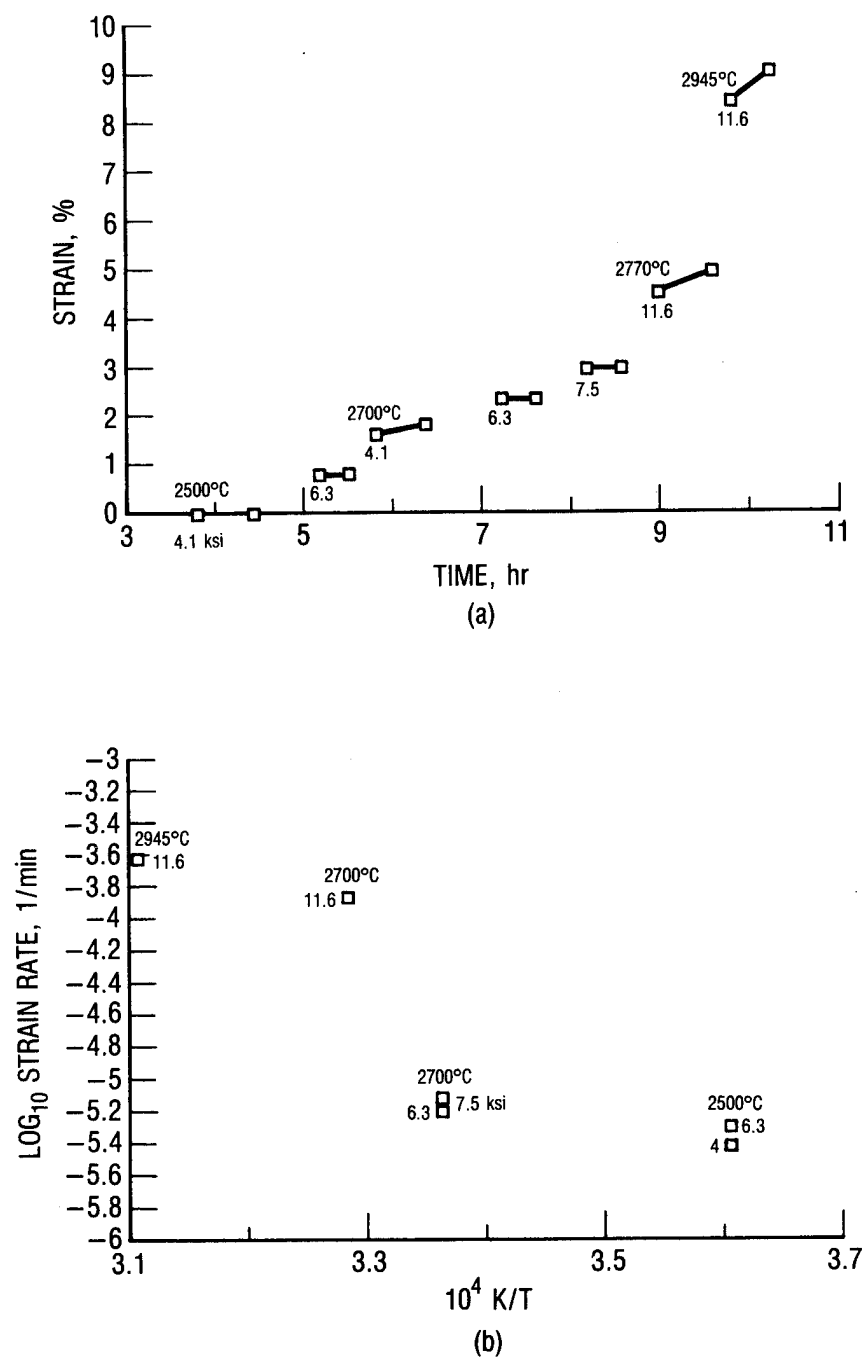


Fig. 6. Plots of (a) Creep Data from Low to High Temperature and (b) Activation Energy, for HM3000/15V Composites

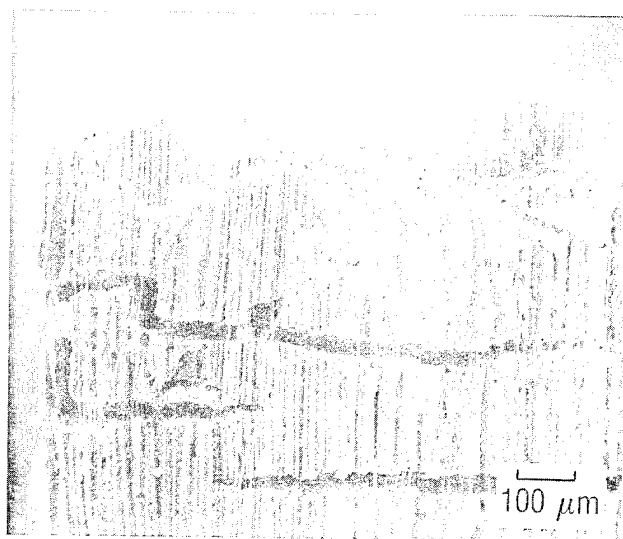
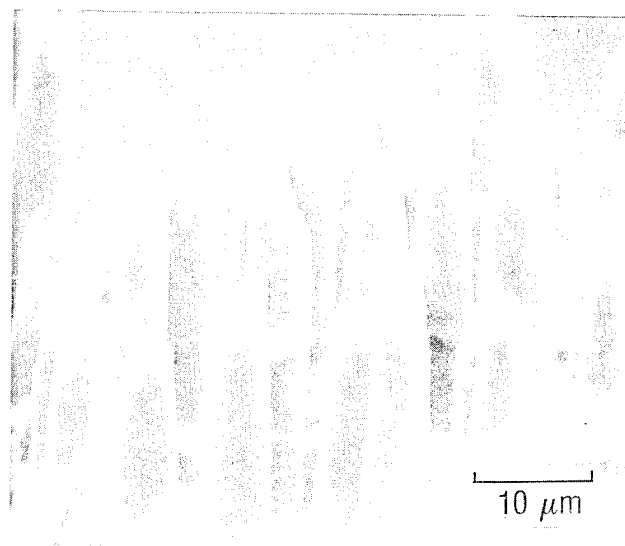


Fig. 7. Photomicrographs of Failed End of HM3000/15V Specimen, Showing Filament Necking and Matrix Shrinkage Cracks

B. VARIABILITY OF CREEP

The creep strains to failure of the three different composite types, WCA/A240, P55/A240, and HM3000/15V, appear to vary considerably. The ways in which they vary indicate some of the important differences in composite properties that arise from the differences in properties of the composite constituents. Creep in WCA/A240 (Fig. 3a) begins to be appreciable at about 2200°C, as indicated by the increasing changes in the LVDT readings (Table 1). Nominal filament diameter for WCA is 9 μm , with 1440 filaments/yarn. A steadily increasing elongation rate is observed as temperature increases to about 2420°C. A slight decrease in temperature (as measured by the optical pyrometer) occurred at 2420°C because of a slight shift in the position of the sample in the furnace: The sample moved slightly away from the automatic pyrometer target zone, resulting in a small temperature excursion ($\Delta T \approx -70^\circ\text{C}$), which caused a marked decrease in the elongation. The load was increased, in increments of 50 g, to 273 g from an initial 173 g. Significant creep did not resume until the temperature had been increased again to 2390°C, only 30°C below the temperature at which a noticeable creep rate was previously observed at a load of 173 g. The elongation rate did not surpass the rate observed at the earlier load until the temperature had exceeded 2420°C. Thus, in this instance, the creep rate does not have a simple functional dependence on temperature and load only; it depends in a more complex way on the prior loading and heat-treatment history. The data suggest that, typically, the elongation rate at a given load and temperature is decreased by prior heat temperature and elongation at the same or a higher temperature. The variation of thermal expansion characteristics of carbon fibers (Thornel 50, Thornel 75, and CX2) with temperature and number of cycles has been observed (Lowe, 1975) under small tensile stresses (one to two orders of magnitude smaller than the stresses used in this study). However, the data obtained in this study indicate that similar time-, temperature-, and stress-dependent changes also occur in the fibers in a unidirectional composite.

For temperatures above 2390°C, creep rates were observed to increase steadily with temperature until failure occurred. No further examination was made of the range of elongation rates as affected by prior deformation at

higher temperatures, because of the experimental difficulty of repeating measurements over using manual temperature adjustments, and because of the long times required to repeat the measurements.

Figure 3b shows an activation energy plot of logarithmic creep rate as a function of inverse absolute temperature. Activation energy is taken to be the slope of the straight line fit through the data points, in accordance with the expected temperature dependence of creep at high temperature [see Eq. (3), p. 18]. All rates correspond to a 173 g load. The activation energy of 135 kcal/mole is somewhat higher than the values obtained for impregnated WCA yarn (Feldman, 1983), although, as mentioned above, measured creep rates are not a strict function of stress and temperature alone. The presence of the matrix generally reduces the fiber creep rates to below those in the same fiber in the unimpregnated form. Another indication of the difference in stress behavior between the composite and unimpregnated yarn bundles is that the yarn bundles tend to fail filament by filament as the final point of failure is approached. This form of failure promotes a tertiary creep region (Hayden et al., 1965), where the creep rate begins to accelerate as more and more filaments fail, placing the remaining filaments under greater stress and causing them to creep at a higher rate (Feldman, 1983, 1985). Substantial necking of filaments was also observed at the broken ends.

In contrast, sudden fracture tends to occur at higher temperatures in the matrix-impregnated yarn samples, and the fracture runs completely across the sample at a single location. This marked difference in impregnated-versus-unimpregnated-yarn fracture behavior, observed in all three composite systems, indicates that the matrix is a crucial element in transferring stress between filaments. A break in a filament can enhance the local stress more in neighboring filaments when there is stress transfer by the matrix than when there is not (Hull, 1981). Different deformation processes of matrix and fiber may introduce a composite activation energy for creep different from that of the fiber alone. Transfer of stress between fibers is achieved through the matrix, and the activation energies for creep of the matrix and filaments is expected to differ, since the two components have different degrees of preferred orientation, crystallinity, cross-linking, etc.

Figure 4a presents the data for the P55/A240 sample. The segments of rapid temperature increase (left unconnected), with their more vertical slopes, can be distinguished from segments of constant temperature, with their more horizontal slopes. The data shown are at a constant load of 273 g, corresponding to 2.5 ksi for P55, assuming the tensile load is carried predominantly by the filaments ($D = 10 \mu\text{m}$, $N = 2000$). Compared with the WCA/A240 data, the total apparent elongation to failure is small. The apparent activation energy of about 108 kcal/mole (Fig. 4b) is higher than that observed for impregnated P55 (Feldman, 1983). One factor contributing to the differences between P55 and WCA is likely the WCA fiber's lower degree of preferred orientation, so that further "dewrinkling" occurs in the fiber before the layer planes are almost straight and other deformation mechanisms manifested, such as basal plane slippage or mass transport by vacancy diffusion within the basal planes. Typically, the impregnated yarn samples have been found to survive the creep testing to higher temperatures. The creep rate measurements of the impregnated yarns tend to reflect a higher temperature range than those obtained for the unimpregnated yarn. Thus, higher temperature creep mechanisms, with slightly higher activation energies, are observed.

Other factors determining creep behavior in unidirectional composites are related to fiber-matrix interaction and stress transfer, which will be influenced by differences in the surface structure (i.e., roughness, crystalline orientation) of the fibers and their influence on bonding. Figure 8 displays the surfaces of WCA and P55 carbon filaments for comparison. There are noticeable differences in the degree of surface roughness or crenulation, indicating that greater roughness should contribute to the degree of matrix-filament bonding and interaction.

In Fig. 6a, the creep data versus time for HM3000/15V are plotted. The nominal filament diameter for HM3000 is $7 \mu\text{m}$, with 3000 filaments/yarn. The sample was cooled by reducing the furnace temperature prior to failure on the first cycle and then reheated to ascertain the creep behavior on the second heating cycle. The creep is essentially negligible at temperatures below the previous maximum temperature attained (2700°C , 7.7 ksi stress). Thus, the

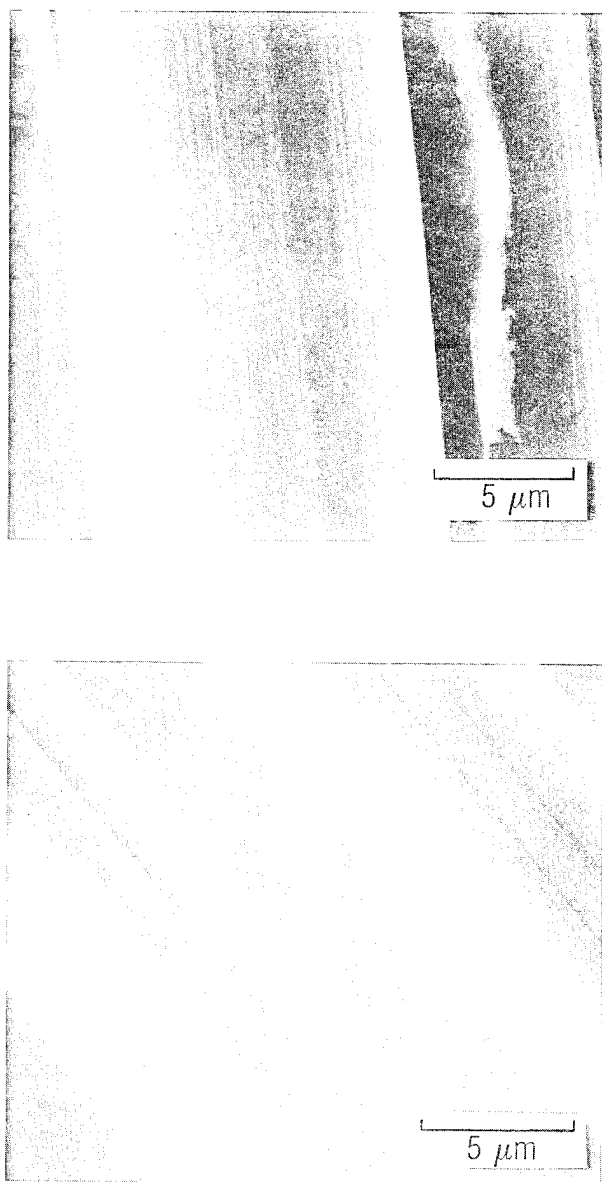


Fig. 8. Photomicrographs of Surface Geometry of P55 (Round) and WCA (Crenulated) Carbon Filaments (As-received), for Comparison

creep behavior depends on prior heat-treatment history and on temperature and stress, because high-temperature- and stress-induced changes, such as de-wrinkling of basal layers in fibers, increased graphitization of matrix and fiber, and cracking. The effects of heat-treatment history on mechanical behavior have been documented for many other forms of carbon and graphite (Kelly, 1981).

In Fig. 6b the logarithm of the strain rate is plotted versus inverse absolute temperature, the same as for the preceding materials. An overall straight-line fit through the data would give approximately 120 kcal/mole; however, we have not calculated activation energies in this case, because the stresses vary for most of the points. Stress levels were varied to study the effect of stress changes on the creep rate. As a result, not enough creep rates at constant stress levels were obtained to get activation energies for the entire set of data. At the two lower temperatures, 2500 and 2700°C, there is some indication of an increase in the strain rate caused by increases in the applied stress level.

The total elongation of the unidirectional composites can be understood in terms of differences in fiber properties and is largely independent of the matrix. In order of increasing elongation, the three composites described, HM3000/15V, P55/A240, and WCA/A240 (1.3%, 2.6%, and 20.7% total elongation to failure, respectively), contain different carbon fibers and different matrices. Fibers with higher modulus and substantial preferred orientation exhibit lower total elongation. The lowest elongation composite, HM3000/15V, contains HM3000 PAN-based fibers, which have a fine crystallite structure with some degree of cross-linking, or entanglement, between the ribbonlike basal plane layers of the crystallites (Donnet and Bansal, 1984). In the P55/A240 composite, although the P55 fiber has a modulus comparable to that of HM3000, it is more graphitizable; therefore, its structure is less glassy and is cross-linked, which more easily accommodates slip and deformation between the basal planes, as well as similar deformation mechanisms manifested in other fibers. In the WCA/A240 composite, the WCA fiber is a lower modulus material that has both a low degree of graphitic order and a relatively low preferred orientation. It can undergo a greater degree of further alignment of the crystallites before failure than the other two fibers. Thus, elongation to

failure is dominated by the fiber properties and is not strongly affected by the differences in matrix, although properties other than total elongation, such as toughness, fracture behavior, and flexural stiffness, are more influenced by matrix properties.

The dependence on stress and temperature of the creep rate in carbon fibers, as well as in a large range of other materials, is described according to (Hawthorne, 1976)

$$\dot{\epsilon} = A \sigma^n e^{(-E/kT)} \quad (3)$$

where $\dot{\epsilon}$ is the creep rate, A is a constant, σ is the stress, n is a stress exponent, E is the activation energy, k is Boltzmann's constant, and T is absolute temperature. The stress exponent is determined from the expression

$$n = \frac{\log (\dot{\epsilon}_1 / \dot{\epsilon}_2)}{\log (\sigma_1 / \sigma_2)} \quad (4)$$

For example, based on stress changes at 2500°C for HM3000/15V (Fig. 6b), from 647 to 6.3 ksi (assuming the fiber bears the entire load and the matrix serves only for stress transfer), the value of n is 1.4, corresponding approximately to simple viscous behavior (which requires a strain rate proportional to stress). Although the composite yarn appears to have fairly low stress dependence compared with that of unimpregnated yarns, additional data are needed to assess more fully the stress dependence of creep.

C. THERMAL EXPANSION EFFECTS

1. MEASUREMENTS

Because thermal expansion is the major contributor to sample elongation during periods of rapid temperature change [i.e., the first term to the right in Eq. (2) is greater than the second term], the thermal expansion of the composite during temperature changes between isothermal periods can be estimated from the sample elongation. The approximate analysis yields results that are within the expected range and necessarily includes some contribution

to the thermal expansion from portions of the sample along the load train other than the sample, such as sample supports and connectors at the ends. Since such contributions are the same for each sample, the differences in thermal expansion behavior between different composite samples are more significant than absolute magnitudes.

The coefficient of thermal expansion (CTE), α , relates sample strain to temperature changes as follows:

$$\epsilon = \alpha \Delta T \quad (5)$$

where ϵ is the thermal strain and ΔT is the temperature change. The furnace temperature can be approximated along the length of the tube by assuming (Feldman, 1985) a parabolic temperature distribution of the form

$$T(x) = T_{\max} (1 - x^2) \quad (6)$$

where x (dimensionless) is position-normalized by the sample length. The incremental temperature along the furnace is

$$\Delta T(x) = \Delta T(1 - x^2) \quad (7)$$

for an increase ΔT in the maximum temperature T_{\max} . The average thermal strain over the length of the sample can be obtained from Eq. (7) as

$$\langle \epsilon \rangle = \langle \alpha \Delta T(x) \rangle = \alpha \Delta T \int_0^1 (1 - x^2) dx \quad (8)$$

Calculating the average strain caused by the temperature increase ΔT by integrating gives

$$\langle \epsilon \rangle = \frac{2}{3} \alpha \Delta T \quad (9)$$

The CTE is estimated from the measured average strain data using Eq. (9) in the form

$$\alpha = \frac{3/2 \langle \epsilon \rangle}{\Delta T} \quad (10)$$

Changes in length for each temperature increment for WCA/A240 are shown in the data in Table 2 in terms of voltage changes recorded by the LVDT. Using an overall sample length, including supports of 914 mm (36 in.), and the LVDT calibration constant of 0.099 V/mm, the thermal strain can be calculated by dividing the voltage change by the LVDT calibration constant and the sample length. The effective thermal expansion coefficient [calculated from Eq. (10)] varies with increasing maximum temperature, between 33.3 and $49 \times 10^{-6}/^{\circ}\text{C}$ between T_{max} of 2200 and 2600°C. If we omit the highest temperature value because of the increasing influence of creep, the average CTE is $40.8 \times 10^{-6}/^{\circ}\text{C}$.

Changes in length for the temperature increments for P55/A240 and HM3000/15V are listed in Tables 3 and 4 in terms of voltage changes in the LVDT transducer output. Effective thermal expansion coefficients are calculated as described above. The effective thermal expansion coefficient of

Table 2. WCA/A240 Thermal Expansion

Time	Temperature, °C	Weight, g	LVDT, V
5:07:30	2099	173	1.8168
5:15	2150		1.9378
α (V/°C): 2.37E-3			
5:45	2200	173	2.1397
5:52:30	2281		2.3465
α (V/°C): 2.55E-3			
6:41:15	2260	173	2.6282
6:48:45	2332		2.7726
α (V/°C): 2.01E-3			
11:48:45	2500	173	1.0546
11:56:15	2600		1.3504
α (V/°C): 2.96E-3			
12:41:15	2620		2.7252
12:45	rising		2.8325
12:48:45	2770		3.2647
α (V/°C): 2.166E-3			

Table 3. P55/A240 Thermal Expansion

Time	Temperature, °C	Weight, g	LVDT, V
4:00	2205	273	1.1540
4:07:30	2338		1.2202
α (V/°C): 4.98E-4			
4:30	2340	273	1.2691
4:41:15	2390		1.3500
α (V/°C): 1.62E-3			
5:03:45	2390	273	1.3671
5:11:15	2480		1.4308
α (V/°C): 7.07E-4			
5:48:45	2490	273	1.5042
6:00	2600		1.5949
α (V/°C): 8.25E-4			
7:03:45	2680	273	1.8398
7:07:30	2760		1.9891
α (V/°C): 1.87E-3			

Table 4. HM3000/15V Thermal Expansion

Time	Temperature, °C	Weight, g	LVDT, V
First Run			
2:15	1905	338	0.3842
2:30	2008		0.4203
α (V/°C): 3.50E-4			
2:37:30	2008	338	0.4203
2:52:30	2050		0.4515
α (V/°C): 7.43E-4			
3:30	2293	338	0.5710
4:00	2500		0.6983
α (V/°C): 6.15E-4			
7:07:30	2650	527	1.0252
7:22:30	2700		1.0596
α (V/°C): 6.88E-4			
Second Run			
1:30	2470	967	1.1073
1:45	2640		1.2170
α (V/°C): 6.45E-4			

P55/A240 varies with increasing maximum temperature, between 8.26 and $46.8 \times 10^{-6}/^{\circ}\text{C}$ over the temperature range 2205 to 2760°C. The average of the measured CTE values, omitting the highest temperature value, is $15.1 \times 10^{-6}/^{\circ}\text{C}$.

The effective thermal expansion coefficient of HM3000/15V fluctuates between 5.8 and $12.3 \times 10^{-6}/^{\circ}\text{C}$ between T_{max} of 1905 and 2700°C. The average CTE, omitting the highest temperature value, is $9.9 \times 10^{-6}/^{\circ}\text{C}$.

2. VARIATION OF THERMAL EXPANSION COEFFICIENTS--DISCUSSION

The apparent CTEs are very high compared with the typical CTE parallel to the basal plane for graphite at high temperature, which approaches $1.2 \times 10^{-6}/^{\circ}\text{C}$ (Reynolds, 1969), although thermal expansion is not usually measured under significant tensile load as in this experiment. This discrepancy can be explained by the fairly large thermal expansion of the parts of the load train other than the sample. Similarly large effective thermal expansion coefficients of carbon yarns have been measured by Lowe (1975) on unimpregnated yarns at high temperatures. Using small loads, he obtained estimated average thermal expansion values between 2200 and 2500°C of from $3 \times 10^{-6}/^{\circ}\text{C}$ for Thornel T50 (Union Carbide, 55 Msi) to $144 \times 10^{-6}/^{\circ}\text{C}$ for CX2 (Polycarbon, 4.8 Msi). These values bracket the range of values recorded in the present experiment for matrix-impregnated composite yarns.

The difference in CTE between two samples can be obtained from two independent measurements by cancelling the constant contribution of the permanent parts of the load train. If the sample CTE is α_s and the CTE of the permanent parts is α_p , with V_s being the ratio of the sample length to the overall load train length and V_p being the ratio of the permanent parts' length to the overall load train length, then the total CTE, α_t , is

$$\alpha_t = \alpha_s V_s + \alpha_p V_p \quad (11)$$

Equation (11) is of the same form as the rule of mixtures for the modulus of a unidirectional composite:

$$\alpha_{s(1)} - \alpha_{s(2)} = \frac{\alpha_{t(1)} - \alpha_{t(2)}}{V_s} \quad (12)$$

Here, the fractional length of the sample, V_s , is 40.6 cm/91.4 cm [16 in./36 in.] ≈ 0.44 . The relative differences using the average CTEs calculated for each unidirectional composite are shown in Table 5.

Table 5. Relative Differences in CTE

Composite 1	Composite 2	Relative Difference
P55/A240	HM3000/15V	$11.8 \times 10^{-6}/^{\circ}\text{C}$
WCA/A240	P55/A240	$58 \times 10^{-6}/^{\circ}\text{C}$
WCA/A240	HM3000/15V	$70 \times 10^{-6}/^{\circ}\text{C}$

The simple analysis gives a difference in average CTE that is large compared with the basal plane expansion of graphite, but not unreasonable in light of Lowe's data (1975). However, if the matrix contributes significantly to the thermal expansion, and if there are other effects caused by the large sample length, the nonuniform temperature across the sample, and the applied tensile stress, then the large values may be more realistic. Note that the relative difference between P55/A240 and HM3000/15V is much smaller than the difference between either one and WCA/A240. The disparity reflects the fact that both P55 and HM3000 are relatively high-modulus fibers with high preferred orientation, and therefore have lower longitudinal expansion than WCA fiber, which is lower in modulus and has lower preferred orientation.

The foregoing discussion illustrates a method of obtaining relative differences in CTE between different composite materials using the experimental apparatus for measuring creep. At present, the change in Young's modulus as a function of temperature at high temperatures has not been determined; consequently, it is not possible to ascertain the contribution, if any, of such a change to the apparent thermal expansion. Thermal expansion data can be obtained on samples during periods of rapid temperature increase; creep can be

measured independent of thermal expansion during periods of steady-state temperature distribution. Whereas differences in the fiber component may govern the thermal expansion behavior, the fiber-matrix interaction may also play a role, as it does in both the high-temperature creep behavior and final fracture behavior of the composite. Further work in this area may provide more information on high-temperature composite thermal expansion behavior and increase our insight into creep behavior as well.

D. VIBRATIONAL MODULUS

Subjecting a unidirectional composite to creep at high temperature creates numerous changes in the fiber, matrix, fiber-matrix interface, microcrack structure, and other individual components in the composite. Such internal changes in turn induce alterations in the properties of the composite as a whole, one of the most important being the elastic behavior of the material. By measuring creep-induced changes in such composite properties as Young's modulus and comparing the results with observed changes in the microstructure, the two aspects can be established. Simple mechanical models can aid in understanding the effects of creep on the composite behavior.

A method is under development in the Materials Sciences Laboratory for measuring the elastic modulus of small samples of single filaments and composite yarns. Using a simple vibrating beam technique, the beam's resonance frequency is measured to determine the modulus. In contrast to other related methods, resonance is excited electromagnetically, rather than piezoelectrically, with an alternating current impressed upon the sample, which is placed in a magnetic field. Details of the method and preliminary results on well-characterized materials are discussed in Appendix B.

In the results for the several samples in Table 6, for which a uniform, well-bonded composite beam was assumed, there are large variations in the apparent modulus. For example, P55/15V and P55/A240 show increases in apparent modulus with different heat treatments, from 10.8 to 17.1 Msi and from 6.3 to 22.7 Msi, respectively, along with varying shrinkage in cross-sectional area. The change in area partly accounts for the modulus increase by allowing more high-modulus fibers per unit cross-sectional area. However, matrix effects, such as alignment of the matrix graphitic structure with the fiber surface

Table 6. Vibrating Beam Technique Results
for Unidirectional Composites

Sample	E, Msi	% ROM	Diam, mm	Density, g/cm ³
P55/15V				
as-impregnated	10.8	56	0.767	1.52
1000°C	17.1	76	0.701	1.23
HM3000/15V				
as-impregnated	11.2	35	0.48	1.52
3000°C creep	1.3	11	0.783	1.38
P55/A240				
800°C	6.3	55	0.977	1.03
2700°C	22.7	126	0.78	1.26
WCA/A240				
2700°C	5.7	---	0.433	1.49

("sheath effect"), may also influence the modulus. The decreasing apparent modulus of some of the composites may be interpreted in terms of decreasing degree of bonding between filaments and matrix caused by high-temperature deformation. That is, the fiber modulus is not expected to vary much as a result of the high temperature and deformation experienced. Changes in fiber-matrix bonding most likely cause the vibrational modulus decrease of HM3000/15V, from 11.2 to 1.3 Msi after strain to failure at 3000°C. One might expect that at 3000°C, the "hot-stretching" of the fibers would cause an increase in fiber modulus through increase in preferred orientation of the fiber's graphitic crystallites. However, if the high-temperature deformation also leads to changes in the matrix microstructure and a decrease in the fiber-matrix bonding, an increase in fiber modulus will not be reflected in a corresponding composite modulus increase. Instead, the flexural stiffness of the composite should decrease. This interpretation is supported by earlier work (Feldman, 1985), which described how such treatment of an HM3000/15V composite caused enough filament-matrix debonding that the creep-deformed sample could actually be bent to a fairly small radius at room temperature, producing, in effect, "ductile" behavior. Further work must be conducted in this area to establish the relationship between interfacial bonding and elastic properties as measured by the vibrational technique.

E. ELECTRICAL RESISTANCE PROPERTIES

The electrical behavior of carbon fibers is one aspect that is microstructure sensitive; that is, it is affected by such factors as degree of graphitic order or disorder, concentration of defects or grain boundaries, and degree of anisotropy or preferred orientation. Changes in fiber microstructure accompany the creep process at high temperature, and thus can be reflected in altered electrical transport properties, such as resistivity and magnetoresistance.

The electrical resistivity of different forms of graphite varies widely, depending, for example, on degree of graphitization or crystallinity, and degree of preferred orientation of basal planes along a particular direction (Spain, 1981). In a previous report (Feldman, 1983), a number of carbon fiber materials were measured to determine their resistivities and resistance ratios at 77 and 300 K, as a function of both heat treatment and high-temperature deformation. Additional measurements of resistivities and resistance ratios have been made to determine whether those factors can be correlated with other effects of high-temperature creep and heat treatment.

The findings were qualitatively similar to those reported earlier (Feldman, 1983). In particular, most of the change in resistance ratio, indicative of the relative graphitic order (Robson et al., 1973), appears to be caused by high-temperature heat treatment and not by high-temperature deformation. For example, P55 and WCA fibers exhibited approximately the same resistance ratios, 1.7 and 1.1, respectively, after heat treatment alone at 2500°C and after creep to failure of the yarn at the same temperature. For WCA, a less graphitizable, high-temperature heat-treated yarn, this represented a negligible change from the as-received resistance ratio, with good high-temperature stability; for P55, however, the increase in the relative graphitic order was substantial--from 1.1 (as-received) to 1.7. Additional measurements have shown that in relative graphitic order at a heat-treatment temperature of 2400°C, HM3000, like WCA, alters little but exhibits a slight increase after heat treatment at 3000°C. A discussion of the measurements and further results are given in Appendix C.

These results show the behavior of the unimpregnated yarns; applying them to the impregnated yarns may aid in determining the relative graphitic order of the composite samples and effects caused by differences of composite deformation at high temperature.

IV. DISCUSSION AND CONCLUSION

Our observations of elongation of P55/A240, WCA/A240, and HM3000/15V composites under creep at high temperatures indicated that WCA/A240 had the largest elongation. The material's low modulus and high-temperature-induced decrease of undulations present (as a result of its being manufactured as cloth) may combine to produce this elongation. Conversely, the lower elongations of P55/A240 and HM3000/15V are explained by the relatively higher modulus of their yarns and the initial straightness of the composites, because they originate as yarns rather than cloth. A possible reason for P55/A240's elongation being higher than that of HM3000/15V may be the greater initial creep relaxation of P55 mesophase-pitch yarns on the first high-temperature cycle (cf. Feldman, 1983). That creep rates, total elongations, activation energies, and high-temperature localized fracture behavior of the yarn composites are considerably different from those of their unimpregnated counterparts reflects the contribution of the microstructure, fiber-matrix interaction, and interfilament stress transfer to these properties.

By incorporating a carbonaceous matrix with the yarn, stress transfer was increased between the carbon filaments and, in turn, decreased the region of stress enhancement at flaws and breaks in the fibers. Lower creep rates resulted at high temperature than for unimpregnated yarn. The mechanism of fiber creep itself appears to be the same in both impregnated and unimpregnated yarns, given similar magnitudes of the activation energies. The degree of filament necking and the appearance of the fracture surface--whether fracture is localized along the sample or filament-by-filament breakage occurs over an extended region--is determined mainly by the presence or absence of matrix and the nature of the fiber-matrix interaction. In both impregnated and unimpregnated yarns, the fiber is the main stress-bearing component; it occupies a substantial volume fraction of the composite and has high modulus and strength. In contrast, the matrix is less well oriented, and generally has lower strength and modulus. Because their modulus is higher than that of the matrix, the filaments bear most of the tensile load in the unidirectional

composites, and they bear the entire load in unimpregnated yarns. Similar mechanisms contributing to creep, including dewrinkling of graphitic ribbons in the structure, slippage along the basal plane, and vacancy diffusion, thus occur in both unimpregnated and impregnated yarns.

The matrix's stress transfer capability is affected by both the microstructure of the matrix and the fiber-matrix interface bond. Stress transfer by the matrix is degraded by the presence of extensive microcracking and details of microcrack orientation within the matrix and by weakening of the fiber-matrix bond. Sonic modulus measurements are influenced by the ability of the matrix to transfer stress between fibers, because weakening of the matrix and interface can lead to lower than rule-of-mixtures moduli in unidirectional composites. Both good and poor fiber-matrix bonding and interfilament stress transfer have been indicated by sonic modulus measurements, according to whether the fiber-matrix interface or matrix load-bearing capability has been degraded as a result of high-temperature creep. For example, on the basis of both sonic modulus measurements and microstructural interpretation, the system HM3000/15V appears to undergo fiber-matrix weakening from high-temperature creep. In contrast, in system P55/A240, the fiber-matrix bonding remains good and the matrix continues to transfer load. These differences are caused in turn by the specific structures of both fiber and matrices, where one matrix may debond in high-temperature creep under shear and normal stresses that develop at the interface, while another matrix may not.

Determination of the fiber-matrix interfacial bonding is an area to be explored further, and is of particular importance in relating simple unidirectional fiber-matrix composites to more complex multidirectional composite structures, composed of an interpenetrating network of unidirectional fiber-matrix bundles with complex stress states developed as a result of thermal expansion and processing history.

Additional work discussed here included estimating thermal expansion along the unidirectional composites by means of a simple thermal analysis model. Rather large apparent thermal expansions were predicted at high temperature under load, but similarly large values of thermal expansion at high temperature

have been reported in the literature. Further results were given for measurements of resistivity and relative resistance ratios at 77 and 300 K for various fibers, as a function of heat treatment. Changes in the ratio give a simple measurement of an effective relative graphitic order parameter, as suggested by other workers, for as-received and heat-treated fibers. This information may be useful for further work as a simple method of characterizing graphitization in multidirectional carbon-carbon composites, by analyzing the net electrical properties of the composite in terms of its components.

V. SUMMARY

This report describes observations on the effects of high-temperature creep on some of the mechanical properties and behaviors of unidirectional carbon-carbon composites. An improved creep apparatus has been developed to permit computer-controlled, shock-free loading of a sample. We find creep behavior is thermally activated, becoming significant at 2000 to 2200°C and increasing with temperature until failure, typically at 2500 to 3000°C. Total elongation to failure is determined primarily by fiber properties in unidirectional composites and unimpregnated yarns; total elongation decreases both with increasing degree of preferred orientation and modulus and with increasing graphitization of the fiber. The matrix serves to transfer stress between filaments, and its presence causes impregnated yarn to fail at higher temperatures than unimpregnated yarn.

Thermal expansion, data for which were obtained from the rapid temperature ramp portions of the experiment, appears to be governed mainly by fiber properties, as opposed to matrix behavior. It is lower for high-modulus, highly oriented fibers than for low-modulus, moderately oriented fibers. Dynamic modulus measurements indicated that creep-induced changes in the composite at high temperature alter apparent flexural stiffness. In certain cases (HM3000/15V), weakening of the fiber-matrix interface bond causes a decrease in stiffness; in others (P55/A240) the stiffness remains high, indicating the integrity of the matrix and that of the fiber-matrix interface bond remain substantially intact. Measurements of electrical resistance ratio show that electrical properties are modified by heat treatment at high temperature, but they are not altered substantially by creep.

The information on and characterization of high-temperature creep behavior in unidirectional carbon-carbon composites will be useful for understanding processing behavior and damage in carbon-carbon composites. Improved understanding of processing phenomena should result in more effective and economical materials.

REFERENCES

- Bacon, R. and W. A. Smith, "Tensile Behavior of Carbonized Rayon Filaments at Elevated Temperatures," 2nd Conf. on Industrial Carbon and Graphite (London, 1965), pp. 203-213.
- Baker, C. and A. Kelly, Phil. Mag. **9**, 927-951 (1964).
- Barrett, C. S., Structure of Metals (McGraw-Hill, New York, 1954).
- Baumeister, T., ed., Mechanical Engineer's Handbook (McGraw-Hill, New York, 1964).
- Bright, A. A. and L. S. Singer, Carbon **17**, 59-69 (1979).
- Donnet, J.-B. and R. C. Bansal, Carbon Fibers (Marcel Dekker, Inc., New York, 1984).
- Feldman, L. A., High-Temperature Creep of Carbon Yarns: First Annual Report, TOR-0083(3728-02)-1, The Aerospace Corporation (5 September 1983).
- Feldman, L. A., High-Temperature Creep of Carbon Yarns and Composites: Second Annual Report, TOR-0084A(5728-02)-1, The Aerospace Corporation (15 July 1985).
- Hawthorne, H. M., J. Mater. Sci. **11**, 97-110 (1976).
- Hayden, H. W., W. G. Moffatt, and J. Wulff, The Structure and Properties of Materials, Vol. III, Mechanical Behavior (Wiley, New York, 1965).
- Hull, D., Introduction to Composites (Cambridge, 1981).
- Kelly, B. T., Physics of Graphite (Applied Science Publishers, London, 1981).
- Littleton, H. E. and C. D. Pears, Mechanical, Thermal, and Nondestructive Characterization of GE-2.2.3, AFML-TR-77-48 (April 1977).
- Lowe, D. L., Carbon Graphite Yarn Characterization -- Carbon-Carbon Constituent Sensitivity Study, GE Reentry and Environmental Systems Division, Quarterly Report, 1 April 1975 to 30 June 1975, Contract No. N60921-75-C-0060, Naval Surface Weapons Center.
- Pears, C. D., "A Technical Note on Yarn Properties That Relate to Processing," Metals and Ceramics Info. Ctr., Current Awareness Bull., Spec. Ed., Carbon-Carbon Composite Materials, Issue #7, Battelle Columbus Laboratories (25 June 1980).
- Reynolds, W. N., Physical Properties of Graphite (Elsevier, 1969).

- Robson, D., F. Y. I. Assabghy, E. G. Cooper, and D. J. E. Ingram, J. Phys. D: Appl. Phys. 6, 1822-1834 (1973).
- Sines, G. and B. J. Cohen, "Stresses During Fabrication of Cylindrically Woven Carbon-Carbon Composites," in Proceedings of Symposium on Thermomechanical Behavior of High-Temperature Composites, ed. J. Jortner (Amer. Soc. of Mech. Eng., New York, 1982).
- Spain, I., "Electronic Transport Properties of Graphite, Carbons, and Related Materials," in Chemistry and Physics of Carbon, Vol. 16, eds. P. Walker and P. Thrower (Marcel Dekker, New York, 1981).
- Spence, G. B. and E. J. Seldin, J. Appl. Phys. 41, 3383-3389 (1970).
- Timoshenko, S., D. H. Young, and W. Weaver, Vibration Problems in Engineering (Wiley, New York, 1974).

APPENDIX A. DESCRIPTION OF EXPERIMENTAL APPARATUS

In the arrangement of the high-temperature furnace for a simple creep experiment, illustrated in Fig. 1 (p. 4), the sample is loaded using a hanging weight, which provides a dead load. The arrangement works well for constant loading, but it is difficult to increase or decrease the load without an abrupt shock to the sample, which may cause damage. It is also not convenient for experiments that may require a variable load on the specimen. A system has been designed and built that enables better control of the load on the sample with an electrical loading device and a feedback controller (Fig. 2, p. 4). The load cell (Precision Load Cell Co. model K2, 0-5 lb) is located at one end of the furnace outside the exhaust flange, and the fixed end of the sample is attached to the load cell. The moveable end of the sample passes through the opposite end of the furnace, where it attaches to the LVDT core. The LVDT core is in turn attached to the movable core of a 110-VDC continuous-duty solenoid (Trombetta Corp. model P-Q 517). The following subsections describe the operation of these components.

A.1. GAIN-OF-20 POWER AMPLIFIER

The solenoid is energized by a gain-of-20 dc power amplifier that is powered by a 100-VDC power supply (Acopian model A100MT130). The voltage level to the solenoid is controlled by the process controller (Research Incorporated) through the gain-of-20 power amplifier. The process controller receives the output signal from the load cell and adjusts the voltage level on the solenoid to maintain a steady load in the range of 0 to 5 lb on the sample. The load setpoint of the controller can also be adjusted by a programming voltage, which permits remote control by a computer.

The amplifier that controls power to the dc solenoid for applying the load to the sample is required to control up to 100 VDC at 500 mA. The circuit is a feedback-stabilized amplifier that uses a high-voltage transistor (RCA 2N6674) to control the final output. A schematic diagram of the amplifier is given in Fig. A-1.

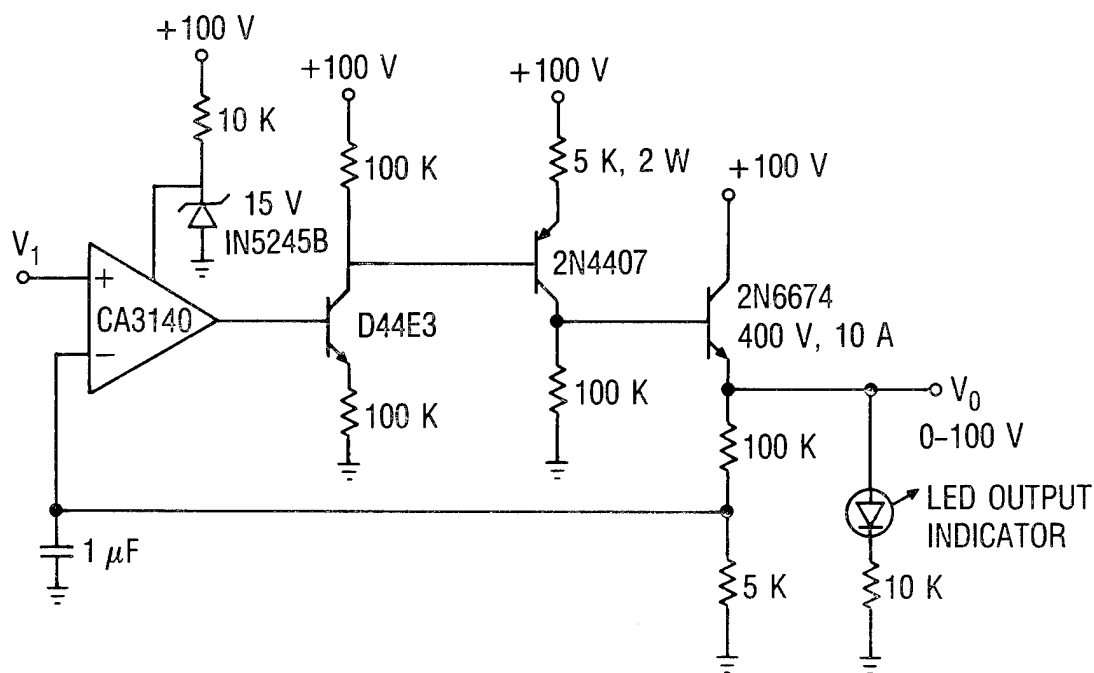


Fig. A-1. Schematic Description of the Gain-of-20 Power Amplifier

A.2. SOLENOID LOAD CONTROL STABILITY

The solenoid is inherently unstable as a constant-load device, because, for a given voltage level, the pulling force increases as the core is pulled into the solenoid and tends to create a runaway condition. That is, a slight movement of the core into the solenoid creates a greater pull, which in turn causes the core to move in further. Figure A-2 shows the force versus displacement curve at a given voltage for the Trombetta solenoid. To overcome this basic instability requires a feedback controller with a load cell to monitor the load and lubrication of the solenoid with a viscous silicone grease to damp the solenoid's response.

The feedback controller can become unstable because of the large inertia of the solenoid core (approximately 500 g), even though the controller can continuously adjust the voltage to the solenoid to maintain a constant pull on the load cell. The sleeve in which the core moves was lubricated with a viscous grease (Dow Corning silicone vacuum grease) to slow the speed of the

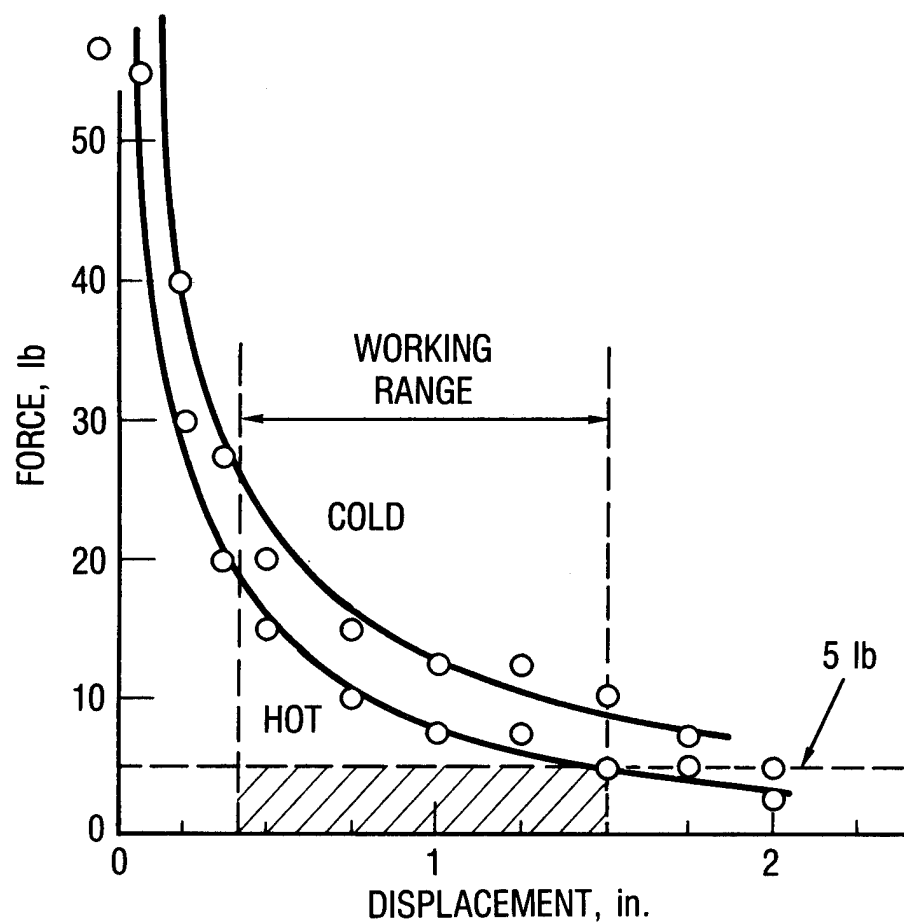


Fig. A-2. Force versus Displacement Curves for Trombetta Solenoid

solenoid core response and avoid having to decrease the gain of the feedback controller. This eliminated the control instability problem. The response to a change in the load setpoint became slower with the viscous grease, requiring up to 30 sec to settle down to a new load level. This was an adequate amount of time for the current experiment, because changing loads during the experiment takes at least several minutes. Another advantage of the slow response is that the load may be changed gently to prevent shock or damage to the sample.

A.3. COMPUTER CONTROL OF LOAD AND TEMPERATURE

A Hewlett-Packard data acquisition/control system, consisting of an HP 85B computer and an HP 3497A data acquisition system, is used to control the experiment and to store and manipulate data. Temperature is controlled by a feedback system using a process controller in conjunction with an IRCON automatic pyrometer. Examples showing both cyclic variation of load on a sample in the furnace and programmed control of temperature are presented in Figs. A-3 and A-4.

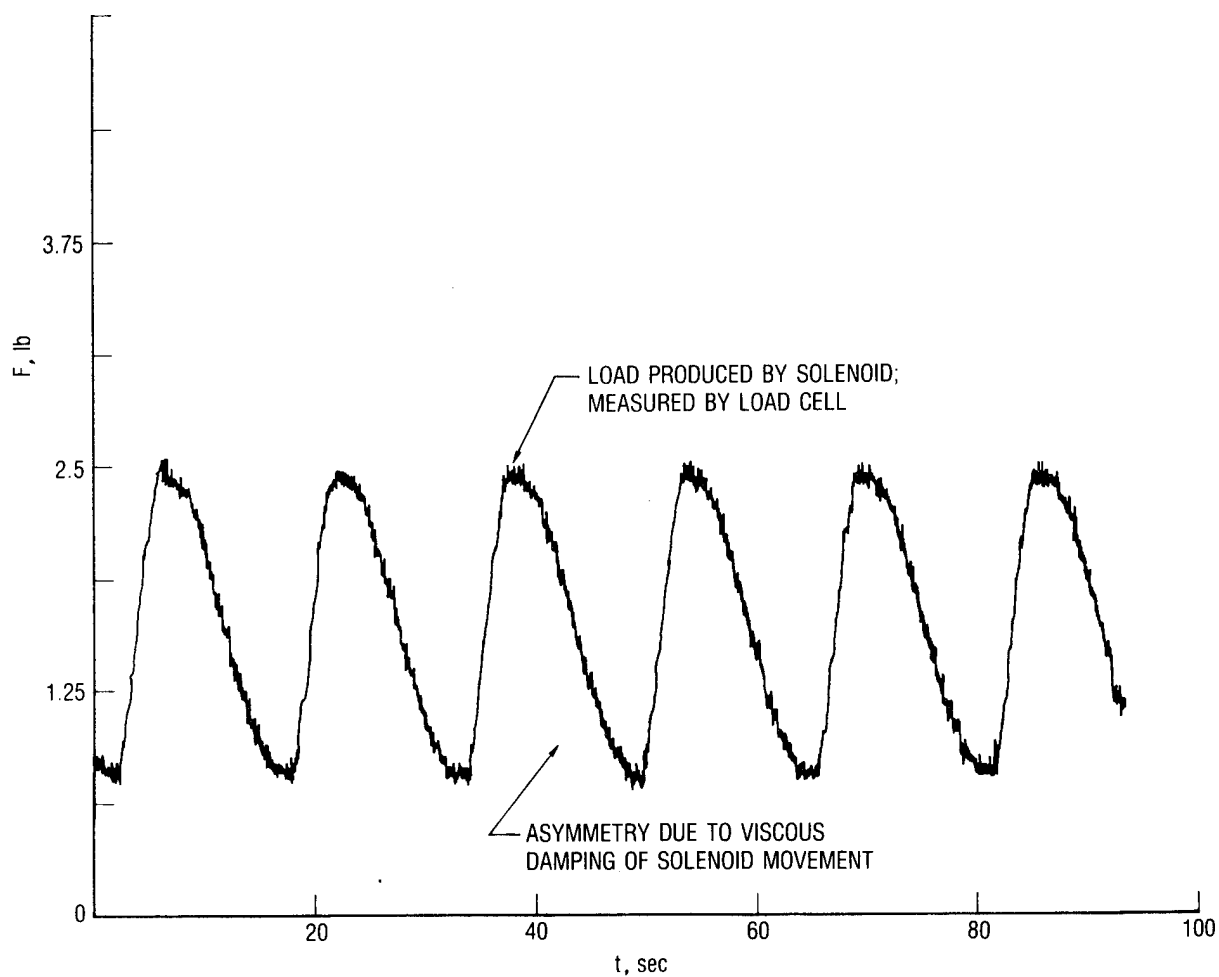


Fig. A-3. Example of Cyclic Variation of a Load on Sample in Furnace

```

10 REM DIALOG
20 DIM V(20)
30 ON TIMER# 1:10000 GOSUB 130
40 DISP "START"
50 DISP "START"
60 N=0
70 GOSUB 460
80 IF N=15 THEN GOTO 80
90 N=N+1
100 GOSUB 460
110 GOSUB 480
120 END
130 REM **OUTPUT ROUTINE**
140 PRINT
150 PRINT N
160 P=18
170 GOSUB 430
180 PRINT V(K); "LOAD PROGRAMMIN
G VOLTS"
190 K=11
200 GOSUB 430
210 PRINT V(K); "IRCON OUTPUT VOL
TS"
220 K=12
230 GOSUB 430
240 PRINT V(K); "SOLENOID VOLTS"
250 K=13
260 GOSUB 430
270 PRINT V(K); "LVDT VOLTS"
280 K=14
290 GOSUB 430
300 PRINT V(K); "DC FURNACE AMPS"
310 K=15
320 GOSUB 430
330 PRINT V(K); "DC FURNACE VOLTS"
340 K=16
350 GOSUB 430
360 PRINT 1000*V(K); "LOAD CELL M
V"
370 GOSUB 460
380 PRINT N*1000; "CH 1 OUTPUT (
LOAD)"
390 GOSUB 480
400 PRINT N*1000; "CH 0 OUTPUT (
TEMP)"
410 N=N+1
420 RETURN
430 OUTPUT 709; "A1";K
440 ENTER 709; V(K)
450 RETURN
460 OUTPUT 709; "A04.1";N*1000
470 RETURN
480 OUTPUT 709; "A04.0";N*1000
490 RETURN

000125 LOAD PROGRAMMING VOLTS
000005 IRCON OUTPUT VOLTS
000015 SOLENOID VOLTS
000004 DC FURNACE AMPS
000004 DC FURNACE VOLTS
000004 CH 1 OUTPUT (LOAD)
000004 CH 0 OUTPUT (TEMP)

1 000127 LOAD PROGRAMMING VOLTS
000005 IRCON OUTPUT VOLTS
000021 SOLENOID VOLTS
000023 LVDT VOLTS
000003 DC FURNACE AMPS
000003 DC FURNACE VOLTS
1000 CH 1 OUTPUT (LOAD)
1000 CH 0 OUTPUT (TEMP)

2 000127 LOAD PROGRAMMING VOLTS
000017 IRCON OUTPUT VOLTS
000005 SOLENOID VOLTS
000023 LVDT VOLTS
000004 DC FURNACE AMPS
000003 DC FURNACE VOLTS
2000 CH 1 OUTPUT (LOAD)
2000 CH 0 OUTPUT (TEMP)

3 000127 LOAD PROGRAMMING VOLTS
000017 IRCON OUTPUT VOLTS
000023 SOLENOID VOLTS
000024 LVDT VOLTS
000001 DC FURNACE AMPS
000003 DC FURNACE VOLTS
3000 CH 1 OUTPUT (LOAD)
3000 CH 0 OUTPUT (TEMP)

4 000127 LOAD PROGRAMMING VOLTS
000017 IRCON OUTPUT VOLTS
000023 SOLENOID VOLTS
000024 LVDT VOLTS
000002 DC FURNACE AMPS
000003 DC FURNACE VOLTS
4000 CH 1 OUTPUT (LOAD)
4000 CH 0 OUTPUT (TEMP)

5 000127 LOAD PROGRAMMING VOLTS
000017 IRCON OUTPUT VOLTS
000023 SOLENOID VOLTS
000024 LVDT VOLTS
000002 DC FURNACE AMPS
000003 DC FURNACE VOLTS
5000 CH 1 OUTPUT (LOAD)
5000 CH 0 OUTPUT (TEMP)

6 000127 LOAD PROGRAMMING VOLTS
000017 IRCON OUTPUT VOLTS
000023 SOLENOID VOLTS
000024 LVDT VOLTS
000002 DC FURNACE AMPS
000003 DC FURNACE VOLTS
6000 CH 1 OUTPUT (LOAD)
6000 CH 0 OUTPUT (TEMP)

7 000127 LOAD PROGRAMMING VOLTS
000017 IRCON OUTPUT VOLTS
000023 SOLENOID VOLTS
000024 LVDT VOLTS
000002 DC FURNACE AMPS
000003 DC FURNACE VOLTS
7000 CH 1 OUTPUT (LOAD)
7000 CH 0 OUTPUT (TEMP)

8 000127 LOAD PROGRAMMING VOLTS
000017 IRCON OUTPUT VOLTS
000023 SOLENOID VOLTS
000024 LVDT VOLTS
000002 DC FURNACE AMPS
000003 DC FURNACE VOLTS
8000 CH 1 OUTPUT (LOAD)
8000 CH 0 OUTPUT (TEMP)

9 000127 LOAD PROGRAMMING VOLTS
000017 IRCON OUTPUT VOLTS
000023 SOLENOID VOLTS
000024 LVDT VOLTS
000002 DC FURNACE AMPS
000003 DC FURNACE VOLTS
9000 CH 1 OUTPUT (LOAD)
9000 CH 0 OUTPUT (TEMP)

10 000127 LOAD PROGRAMMING VOLTS
000017 IRCON OUTPUT VOLTS
000023 SOLENOID VOLTS
000024 LVDT VOLTS
000002 DC FURNACE AMPS
000003 DC FURNACE VOLTS
10000 CH 1 OUTPUT (LOAD)
10000 CH 0 OUTPUT (TEMP)

10 ESH DIALOG
20 DIM V(20)
30 ON TIMER# 1:10000 GOSUB 110
40 DISP "START"
50 N=0
60 GOSUB 430
70 IF N=11 THEN GOTO 70
80 N=N+1
90 GOSUB 430
100 END
110 REM **OUTPUT ROUTINE**
120 PRINT
130 PRINT N
140 K=18
150 GOSUB 400
160 PRINT V(K); "LOAD PROGRAMMIN
G VOLTS"
170 K=11
180 GOSUB 400
190 PRINT V(K); "IRCON OUTPUT VOL
TS"
200 K=12
210 GOSUB 400
220 PRINT V(K); "SOLENOID VOLTS"
230 K=13
240 GOSUB 400
250 PRINT V(K); "LVDT VOLTS"
260 K=14
270 GOSUB 400
280 PRINT V(K); "DC FURNACE AMPS"
290 K=15
300 GOSUB 400
310 PRINT V(K); "DC FURNACE VOLTS"
320 K=16
330 GOSUB 400
340 PRINT 1000*V(K); "LOAD CELL M
V"
350 GOSUB 400
360 PRINT N*1000; "CH 1 OUTPUT (
LOAD)"
370 GOSUB 400
380 PRINT N*1000; "CH 0 OUTPUT (
TEMP)"
390 N=N+1
400 RETURN
410 OUTPUT 709; "A1";K
420 ENTER 709; V(K)
430 RETURN
440 OUTPUT 709; "A04.1";N*1000
450 RETURN
460 OUTPUT 709; "A04.0";N*1000
470 RETURN

```

Fig. A-4. Sample Printout of Programmed Control of Temperature

APPENDIX B. MEASUREMENTS OF FIBER AND COMPOSITE MODULI
BY A MECHANICAL VIBRATION TECHNIQUE

B.1. INTRODUCTION

In the past, simple vibrating cantilever beam experiments were used for measuring the elastic behavior of graphitic materials, including large changes in the elastic properties of highly oriented crystalline graphite caused by irradiation (Baker and Kelly, 1964) and various torsional and vibrational resonances of bars of graphite (Spence and Seldin, 1970). To determine material properties by this technique requires analysis of measurements with the aid of the theory of vibrating beams.

Simple beam theory predicts a series of well-defined frequencies, or modes of transverse vibration, that are a function of elastic modulus, E ; the moment of inertia of the beam cross section, I ; the mass per unit length, ρ ; and the length of the beam, L . Derivations of the necessary formulas are contained in the literature, for example, in Timoshenko et al. (1974). Here, we present the formulas for the frequencies of the lowest vibrational modes of a beam with both ends clamped [Eq. (B-1)] and with both ends simply supported [Eq. (B-2)] (Baumeister, 1964), assuming a suitably long and slender beam such that the frequency is not influenced by the shear modulus (Baker and Kelly, 1964):

both ends clamped

$$f_1 = 3.58 \frac{(gEI)^{1/2}}{(wL^4)^{1/2}} \quad (B-1)$$

both ends simply supported

$$f_1 = 1.56 \frac{(gEI)^{1/2}}{(wL^4)^{1/2}} \quad (B-2)$$

where

EI = flexural stiffness, lb-in. (dyne-cm)
w = weight per unit length, lb/in.
L = length of beam, in. (cm)
g = 386 in./sec/sec (w/g = mass/length = g/cm)

B.2. EXPERIMENTAL

Vibration experiments were performed on samples of Union Carbide mesophase pitch carbon fiber (P55, 55-Msi modulus), National Carbon 0.32-cm- (1/8-in.)-diameter, high-purity graphite spectroscopy rods; Union Carbide ATJ-S fine-grain graphite; and 3-D carbon-carbon composite (GE 2.2.3) (see Figs. B-1 and B-2). Sample vibration was induced by passing a current through the sample in the presence of a magnetic field.

B.2.1 P55 FIBER

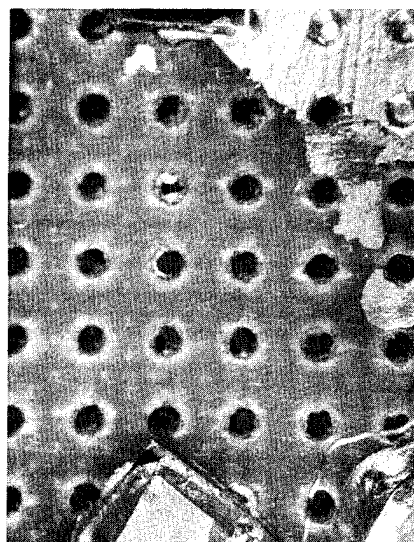
Calculated Modulus

A single filament was cemented at each end to copper contacts by silver paint. The sample was considered to be a beam with both ends clamped. A typical experiment gave the following results from Eq. (B-1):

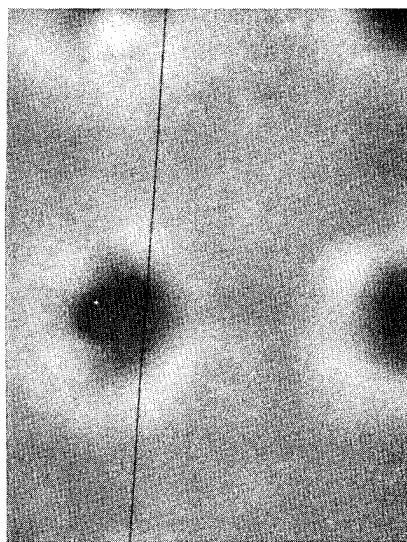
Length (cm)	1.544
*Diameter (μm)	10.4
**Density (g/cm^3)	2.0
Frequency (Hz)	546
Modulus (Msi)	56.7

* Estimated by viewing under optical microscope (nominal diameter provided by Union Carbide is 10 μm).

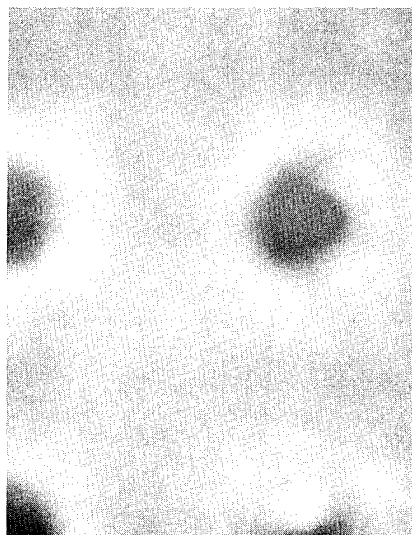
** Measured by methanol immersion.



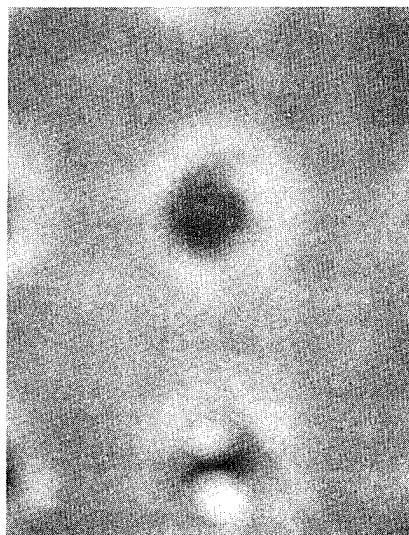
(a)



(c)



(b)



(d)

Fig. B-1. Vibrating P55 Carbon Filament: (a) view of supports and filament in fundamental mode, higher magnification; (b) filament at rest; (c) filament in fundamental mode; and (d) filament simultaneously in fundamental mode and next higher mode (note appearance of node at center of photograph).

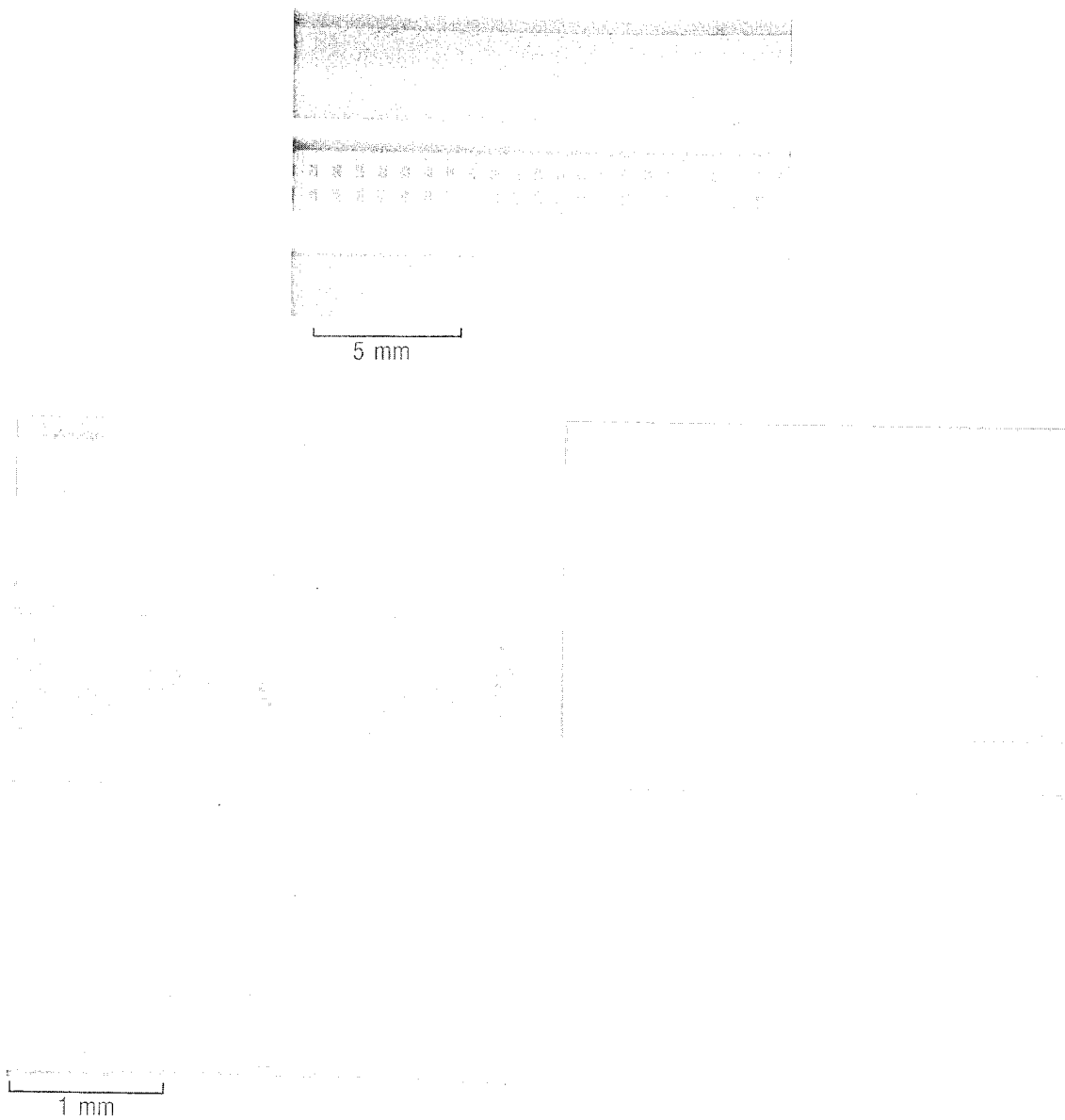


Fig. B-2. Several Carbon Beam Samples, Shown at Rest and in Vibration

The samples discussed below were measured using pointed steel contacts to support the sample at each end. The sample ends were free to pivot against the contacts (zero end moment), and the samples were treated as beams with simply supported ends, according to Eq. (B-2).

B.2.2 ATJ-S FINE GRAIN GRAPHITE (ACROSS GRAIN)

A sample cut across the grain from Union Carbide ATJ-S fine-grain graphite was tested.

Calculated Modulus

A typical experiment gave the following results from Eq. (B-2):

Length (cm)	6.537
b (cm)	0.2044
h (cm)	0.204
Mass (g)	0.4926
Frequency (Hz)	457
Modulus (Msi)	1.18

The 1.18-Msi modulus falls within the range of accepted values of modulus for ATJ-S fine-grain graphite across the grain.

B.2.3 GE 2.2.3 CARBON-CARBON COMPOSITE

A sample cut from a billet of GE 2.2.3 carbon-carbon composite (billet No. 365) parallel to the x-direction was tested. The material is described as having been produced from a Thornel 50 yarn preform with two yarns at each x and y site and three yarns at each z site, with z yarn spacing at 0.076 cm (0.030 in.) and x and y yarn spacing at 0.084 cm (0.033 in.) (Littleton and Pears, 1977). The sample was a beam of rectangular, almost square, cross section, as for the ATJ-S sample.

Calculated Modulus

A typical experiment gave the following results from Eq. (B-2):

Length (cm)	6.7	Length (cm)	6.7
b (cm)	0.206	b (cm)	0.206
h (cm)	0.204	h (cm)	0.204
Mass (g)	0.4971	Mass (g)	0.4857
Frequency (Hz)	1163	Frequency (Hz)	1189
Modulus (Msi)	8.27	Modulus (Msi)	8.45

The 8.27- and 8.45-Msi moduli fall within the range of typical values of modulus for GE 2.2.3 along the x-direction.

B.3. CONCLUSION

Measurements with the vibrating beam method using rather simple equipment have given good results. The method has the potential to be used profitably on graphite, carbon, and carbon-carbon composites as well as on other materials.

APPENDIX C. RESISTIVITY AND RELATIVE RESISTANCE MEASUREMENTS ON CARBON FILAMENTS

C.1. INTRODUCTION

Investigators have studied the electronic properties--e.g., conductivity, magnetoresistance, electron spin resonance, and thermoelectric power--of some types of carbon fibers to determine whether those properties are correlated with the structure of the materials and the effects of processing on them. Measurement of resistivity ratio offers a convenient and simple measurement for carbon fibers that does not require accurate dimensional measurements of individual carbon filaments. The results obtained are also relatively precise and reproducible.

Resistivity measurements have been made by Bright and Singer (1979) on mesophase pitch fibers and by Robson et al. (1973) on various PAN-based fibers. Those researchers found that the degree of graphitization, as indicated by x-ray measurements of graphite crystallite size and interlayer spacing, correlated with the heat-treatment temperature and several of the electronic properties, including the ratios of resistivities at ambient and low temperatures. Bright and Singer (1979) measured the resistivity ratio, $\rho(4.2 \text{ K})/\rho(T)$, as a function of temperature between 4.2 K (liquid-helium temperature) and 300 K (room temperature). Robson et al. (1973) measured the single resistivity ratio, $\rho(77 \text{ K})/\rho(300 \text{ K})$, and found the correlation between graphitic order and the resistivity ratio to be very good. They chose the ratio $\rho(77 \text{ K})/\rho(300 \text{ K})$ to represent empirically the "relative graphitic order" parameter.

C.2. EXPERIMENTAL

Measurements of the resistivity and the resistance ratio, $R(77 \text{ K})/R(300 \text{ K})$, were performed on individual filaments of carbon fiber using a measuring jig constructed of glass-epoxy perforated circuit-board material, with standard push-in terminals as contacts. Filaments approximately 2.5 cm (1 in.) long were secured to the contacts by silver conductive paint. Resistance was measured using a digital ohmmeter (5-digit accuracy). Two-probe

resistance measurement was used, which was deemed adequate to achieve better than 0.1% accuracy, because the total lead wire and contact resistance was less than 1 ohm, whereas the typical sample resistance was several hundred to several thousand ohms. Four-probe measurements were tried in a few cases and agreed with the simpler two-probe measurements. Resistance measurements were not significantly affected by resistive self-heating. They were found to be relatively constant in the range of applied voltage from 0 to 1 V. The apparent resistance decreased slightly at higher voltages, probably because of increased power dissipation associated with self-heating, and also due to changes in resistivity on heating. The applied voltage for most measurements was approximately 0.1 V.

Resistivity was computed from the expression

$$\rho = \frac{Ra}{L} = \frac{\pi d R^2}{4L}$$

where the measured sample resistance is R , length is L , and average diameter is d . Resistance ratio was determined by measuring the sample resistance first at room temperature (typically 300 K) and then after immersion in boiling liquid nitrogen (77 K).

The relative resistance, or resistance ratio, between 300 and 77 K, is reported here rather than the resistivity ratio as in earlier studies (Bacon and Smith, 1965; Feldman, 1983), because the resistance measurements do not have to be corrected for sample dimensions. This is demonstrated by the relation between relative resistance and resistivity ratio,

$$\frac{\rho_1}{\rho_2} = \left(\frac{R_1}{R_2} \right) \left(\frac{d_1^2 l_2}{d_2^2 l_1} \right)$$

The factor $(d_1^2 l_2 / d_2^2 l_1)$ relating the two ratios depends on the sample dimensions at the two temperatures, which differ slightly due to thermal expansion. For example, for an isotropic coefficient of thermal expansion of $10 \times 10^{-6}/^\circ\text{C}$, the percentage difference between the two ratios would be approximately 0.2%. Thus, although the difference is small, it seems

preferable to use the relative resistance and avoid having either to measure the sample dimensions as accurately as the sample resistance or calculate in detail the effects of thermal expansion. The latter would require an extensive consideration of the theoretical and experimental treatment of the thermal expansion of single-crystal and polycrystalline graphite (Kelly, 1981).

C.3. RESULTS

Resistivity measurements at room temperature were made on several fibers and agreed fairly well with manufacturer's specifications. Some changes were observed after heat treatment of the fibers to high temperature. Results are indicated in Table C-1.

Table C-1. Single-Filament Resistivities

WCA (as received):	2443, 2273 $\mu\Omega$ -cm
P55 (as received):	750, 781, 789, 808 $\mu\Omega$ -cm
Post-tensile failure (2500°C):	139, 215, 216 $\mu\Omega$ -cm
Post-heat treatment, no load:	201, 253, 258 $\mu\Omega$ -cm
P100:	912, 302 $\mu\Omega$ -cm

The nominal value of resistivity at room temperature for P55 (VSB-32) is $782 \pm 21 \mu\Omega$ -cm. The decrease in resistivity with heat treatment of the P55 fiber agrees with the observations in the previous report (Feldman, 1983) that the relative resistance also changed markedly with heat treatment for P55 fibers.

Relative resistances, $R(77 \text{ K})/R(300 \text{ K})$, are shown in Table C-2, including those presented in the previous report, where they were referred to as "resistivity ratios," following Robson et al. (1973) and Bright and Singer (1979). Note that measurements on similar fibers appear to be generally reproducible within about 2%. The results are summarized in Table C-3.

Table C-2. Relative Resistance Values for Carbon Fibers

Fiber	As-Received	Creep, 2500°C	Heat-Treated Temperature, °C			
			2400	2500	2700	3000
HM3000	1.157, 1.171 mean: 1.164		1.156, 1.176 mean: 1.166			1.34, 1.347, 1.356 mean: 1.348
WCA	1.08	1.082, 1.087		1.083, 1.085		
P55	1.114, 1.116	1.66, 1.662		1.676, 1.667	1.783, 1.831	
P100	1.46, 1.478, 1.488 mean: 1.475 s.d.: 0.0142		1.71, 1.72	1.675, 1.684 1.697, 1.70, mean: 1.698 s.d.: 0.0165		
	1.57, 1.584, 1.592 1.592, 1.62 mean: 1.5916 s.d.: 0.0182					
	1.698, 1.706, 1.708 1.709, 1.732 mean: 1.7106 s.d.: 0.0127					
P120	1.65, 1.68					
Thornel 300	1.13, 1.15					
HOPG	1.55, 1.80					

Table C-3. Summary of Relative Resistance Values

Fiber	Relative Resistance
WCA	low
P55	increasing with heat-treatment temperature (HTT)
P100	increasing with HTT, decreasing variability
P120	high
Thornel 300	low
HOPG	high (high variability)
HM3000	low--some increase at highest temperature

A higher relative resistance (or resistivity ratio) indicates a greater degree of graphitic order. As discussed in the previous report, x-ray diffraction measurements indicate some increase in graphitization by a decrease in the $d(002)$ lattice spacing toward the ideal crystalline graphite value. Most of this change appeared to be caused by high-temperature heat treatment rather than by the effects of stress and deformation. There was little evidence for significant increase in preferred orientation of the fibers. The results for each fiber type are summarized below.

WCA--Remained at the same low level of relative graphitic order after high-temperature treatment, with or without deformation. This is in agreement with the x-ray diffraction indication of low graphitic order, and the fact that the material was processed at high temperature originally.

P55--Showed a marked increase in resistance ratio with heat treatment, little or no effect due to deformation. X-ray diffraction (see Feldman, 1983) demonstrated increasing graphitization by a decrease in the c-spacing.

P100--High modulus (100-Msi) mesophase pitch fiber. Evidenced some increase in resistance ratio with heat treatment, with substantially higher values as received for P100 than for P55. An interesting observation from the small group of measurements reported here is that the ratios for as-received samples cluster around three values at approximately 1.5, 1.6, and 1.7; the standard deviation was about ± 0.02 , and no measurements fell in between these values. The means of the clusters differ from each other by about 10 standard deviations. One possible reason for these three distinct groups is inherent variability in the material as processed, due to the variable makeup of the pitch precursor, which is a low-cost by-product of petroleum refining. The variability may be due to the presence of a variety of fiber microstructures for the as-received P100 fibers, such as radial, random, etc., as observed in other pitch fibers (Feldman, 1983). Initial observations in the SEM have not revealed obvious differences in structure that would account for a difference in properties. The resistance ratios after heat treatment to 2500°C clustered closely around a single value of approximately 1.7, indicating that whatever differences existed in the fibers previously have been removed, and possibly the properties are not as sensitive to the variations in raw materials after exposure to temperatures around 2500°C as in the as-received condition.

P120--High-modulus (120-Msi) mesophase pitch fiber. The limited number of samples measured had resistance ratios near 1.7, similar to the value for P100 after heat treatment to 2500°C.

Thornel 300--This PAN II fiber of 35-Msi modulus manifested resistance ratios similar to WCA (low-modulus rayon precursor) and P55 as received. The similarities may be due to the relatively low graphitization achieved in PAN precursor fiber.

HOPG--Measurements on highly graphitic, oriented pyrolytic graphite indicated high resistance ratios, about the same as those in high-temperature heat-treated mesophase pitch fibers. Resistance measurements on the HOPG

samples tended to be somewhat indefinite and irreproducible after thermal cycling to liquid-nitrogen temperature, as a result of the easy cleavage, cracking, and delamination of the material. Each resistance ratio given is for one single cycle of measurement at room temperature and in liquid nitrogen.

HM 3000--This PAN I fiber, of 55-Msi modulus, showed resistance ratios as received similar to WCA (low-modulus rayon precursor), Thornel 300, and P55 as received. It was noted that the ratio increased slightly after heating to very high temperature ($>3000^{\circ}\text{C}$). However, it still did not reach as high a value as observed for mesophase pitch precursor fibers.

C.4. CONCLUSION

The observations on the resistance ratios of various fibers reflect the differences in graphitic order between them and the increased order in the more graphitizable materials after heat treatment. They also reveal a very minor effect of deformation at high temperature on the resistance ratio, in general agreement with x-ray diffraction results. Possible further applications of these results to composites may be made by machining slender beams from processed composites and measuring their resistance ratio. That ratio gives a measure of their "relative graphitic order," which may be correlated with various aspects of the processing.